Modular Comprehensive Modeling of Plasma Behavior in Hall Thrusters

IEPC-2019-147

Presented at the 36th International Electric Propulsion Conference
University of Vienna • Vienna, Austria
September 15-20, 2019

Farbod Faraji[1], Maryam Reza[2], Tommaso Andreussi[3]
SITAEL S.p.A., Via A. Gherardesca 5, 56121 Ospedaletto (Pisa), Italy

Abstract: The complex and multiscale nature of the phenomenon of anomalous electron cross-field transport in Hall thrusters has long hindered the development of a self-consistent predictive model for these devices. To achieve this aim, an ideal simulation model should, in principle, resolve a wide range of temporal and spatial scales in a 3D3V phase space, in an extended Hall thruster domain. However, the computational cost of this model is significantly prohibitive for practical applications. In this paper, we present a novel framework to effectively capture the multiscale nature of the phenomenon at remarkably reduced computational cost. A modular simulation model is developed in which each module captures a specific part of the overall complex picture of the problem and interacts iteratively with other modules to provide an almost self-consistent physical description of the electron transport and plasma behavior. Various modules are described in this paper, with a specific focus on the newly-developed Stability Analysis Module (SAM) and its interactions with the Unified Anomalous Transport Code (UATC). Using SAM, the stability of the plasma in the ionization and acceleration regions of two 5 kW-class Hall thrusters with different magnetic field topologies and channel geometries are studied. In the ionization region, low-frequency unstable modes corresponding the spoke instability of various mode numbers are found in both thrusters. In the acceleration region, unstable axial modes with similar characteristics to those of the beam-plasma instability and transit-time instability are observed in the two thruster configurations. Based on these results, the stability of the plasma in the two thrusters are compared, and possible implications related to the cross-field transport are discussed.

Nomenclature

v_{an}	=	anomalous collision frequency
$\langle E_x \rangle$	=	average axial equilibrium electric field
E_x	=	axial equilibrium electric field
k_x	=	axial wave number
k_z	=	azimuthal wave number
L_c	=	channel length
A	=	coefficient matrix
ω	=	complex frequency
φ	=	electric potential
u_{ex}	=	electron axial velocity
u_{ez}	=	electron azimuthal velocity
ω_{ce}	=	electron cyclotron frequency
m_e	=	electron mass

[1] Electric Propulsion Engineer, farbod.faraji@sitael.com
[2] Electric Propulsion Engineer, maryam.reza@sitael.com
[3] Technical Manager, tommaso.andreussi@sitael.com

ω_{pe}	=	electron plasma frequency
p_e	=	electron pressure
T_e	=	electron temperature
$\overrightarrow{u_e}$	=	electron velocity vector
σ_{en}	=	electron-neutral collision cross-section
ν_e	=	electron-neutral collision frequency
n_{n0}	=	equilibrium neutral number density
n_0	=	equilibrium plasma number density
$\widetilde{\Psi}$	=	general representation of fluctuation amplitudes
Φ^*	=	general representation of normalized parameters
ψ'	=	general representation of perturbed plasma parameters
ω_i	=	imaginary frequency component
V_{di}	=	ion axial drift velocity
u_{ix}	=	ion axial velocity
u_{iz}	=	ion azimuthal velocity
m_i	=	ion mass
c_s	=	ion sound speed
T_i	=	ion temperature
$\overrightarrow{u_i}$	=	ion velocity vector
σ_i	=	ionization cross-section
ν_i	=	ionization frequency
R_c	=	mid-radius of thruster channel
$\tilde{E}$	=	perturbed electric field
n'	=	perturbed electron (ion) number density
$\vec{x}$	=	position vector
B_r	=	radial magnetic field component
ω_r	=	real frequency component
m	=	spoke mode number
e	=	unit charge
$\widetilde{\boldsymbol{P}}$	=	vector of the perturbed parameters oscillation amplitudes
$\vec{k}$	=	wave number

I. Introduction

The Hall thruster technology today is the propulsion option of interest for a broad spectrum of space mission scenarios. Hall thrusters are highly-efficient devices that provide many advantages in terms of power-to-thrust ratio, lifetime, manufacturing simplicity and operational versatility compared to other electrostatic EP devices. With the emergence of novel near-Earth and deep-space mission scenarios, the interest in the development of Hall thrusters with power levels above 5kW has surged in the recent years. Nevertheless, as the power level increases, the necessity is felt more for a self-consistent numerical design tool. Such a model allows obtaining reliable and accurate predictions of the thrusters' performance, and carrying out parametric studies, typical to the preliminary design phases of the thruster, at a reasonably low computational cost. As a matter of fact, being the current development approach of Hall thrusters heavily test-dependent, the incurred cost and required time to qualify, for instance, a high-power 20 kW Hall thruster, is enormous. In addition, the life testing of Hall thrusters which amounts to continuous firing times on the order of tens of thousands of hours is truly challenging from the financial and scheduling aspects. Finally, the background pressure and electrical effects of vacuum chambers on the performance and behavior of Hall thrusters introduce uncertainties in the results of on-ground performance characterizations and the extent of similarity with the actual performance of the thruster on orbit. All these issues become much more serious for high-power Hall thrusters.

A major hurdle to achieve a design-aiding tool roots in the physics of Hall thrusters' operation that is not yet fully understood. One of the main open questions regarding the underlying physics of these devices pertains to understanding the electrons dynamics, and particularly, the mechanisms that render the rate of cross-magnetic-field diffusion much larger than those predicted by the classical collision theory. This phenomenon, referred to as "anomalous" electron cross-field transport, poses a real challenge to the development of self-consistent simulation models. This is because of the fact that, in principle, the mechanisms behind this phenomenon and the significance of their contribution to cross-field transport can vary temporally within a period of thruster's characteristic current oscillation[1], spatially from the near-anode to near-plume region, and from one operating condition to another. In this respect, however, as a result of some coordinated efforts within the community (e.g. Princeton ExB Workshop 2018), plasma turbulence is currently believed to play the most significant role. A compelling reason for this notion, besides supporting evidence from a great deal of numerical[2,3,4] and experimental[5,6] efforts, is that Hall thrusters belong to the general category of cross-field plasma configurations, which is characterized by strong anisotropy in the distribution of plasma properties, resulting in a non-quiescent nature and giving rise to many instabilities. Nevertheless, the contributions from other suggested mechanisms, such as electron-wall collisions and Near-Wall Conductivity (NWC), cannot be yet totally ruled out since their direct role in cross-field transport of electrons has been demonstrated in certain thruster designs and operating points[1,7]. It has been also numerically shown[1] that the electron-wall collisions act as regulating the excitation of the instabilities, thus affecting also indirectly the turbulence-induced cross-field transport.

Despite the abovementioned complexities of the problem, the large body of work performed on the subject has provided important insights into the nature of principal current-conducting instabilities in three main regions of the Hall thruster domain (ionization, acceleration and near-plume), particularly including the dependencies of instability waves on plasma equilibrium parameters, and the correlations between the axially-induced current and the waves characteristics[8,9,10]. These insights allow derivation of adequate closure models for the fluid system of equations in each of the thruster regions, thus, proceeding towards the development of a simulation model capable of sufficiently-accurate predictions of the discharge current and plasma average properties, and with eventually no need for a non-physical "Bohm parameter" and/or experimentally-obtained ad-hoc mobility profiles. As a matter of fact, we showed in a previous effort[11] that incorporating such closure models and even under simplifying assumptions, it is possible to acquire more accurate, self-consistent predictions of plasma properties.

Based on the promising results of the preceding work, a novel framework can be devised to numerically predict the instability-induced electron cross-field transport in Hall thrusters, and to incorporate the outcome into a fluid simulation model that captures the evolution of plasma parameters in the thruster. More specifically, instead of developing complex simulation models that shall resolve phenomena with orders of magnitude difference in length and time scales, a **modular** simulation model is developed in which each module captures a specific part of the overall complex picture of the problem and interacts iteratively with other modules to provide an almost self-consistent physical description of the electron transport. Such a model, in principle, remarkably reduces the computational cost and thus, well suits performing parametric studies. This modular code also allows evaluating the sensitivity of the results to the introduced assumptions and to the complexity of the physical models in each module. Figure 1 shows the block diagram of the described comprehensive model, **MICaPS** (**M**odular **I**nstability **C**haracterizer **a**nd **P**lasma **S**imulator), to better illustrate the general scheme of the model and the inter-modular interactions.

Before proceeding further, however, it is important to underline few points regarding the standing of the present effort and the proposed model among the research activities currently ongoing on anomalous electron transport, and the approaches being followed towards self-consistent plasma simulations of Hall thrusters.

First, the modular model is currently intended to serve as a design-aiding predictive tool to be used in the preliminary design phases of Hall thrusters of different power levels and magnetic field configurations. This implies that the accuracy requirements are not needed to be very stringent, as it may be required for a model applicable at later stages of the development of a thruster. Nevertheless, the MICaPS approach can cast light on the modifications that may be needed to progress towards a simulation tool that supplements the qualification campaigns. In this respect, the modularity of the model allows introducing the possible improvements in each of the modules separately, without the need for significant changes to the iteration scheme that links the modules. In any case, for the time being, the potential improvements are primarily aimed at maturing the MICaPS to a level that it provides reliable predictions of the thruster performance parameters and plasma properties in different operating conditions, as required in the early design stages.

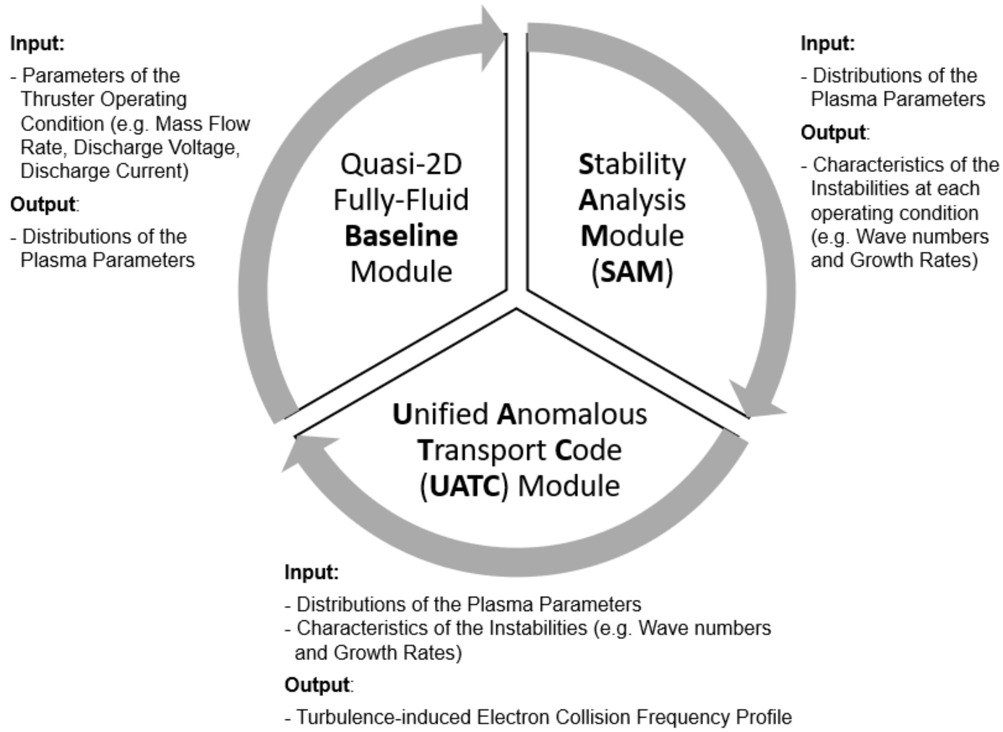

Figure 1: Block diagram of the modular simulation model (MICaPS) with inputs and outputs of each module

In addition, it is also noteworthy that in the similar direction of the MICaPS, there are several other efforts pursued by various researchers to augment the self-consistency of fluid plasma simulations, ranging from the development of first-principles formulations of instability-induced transport[10,12] to incorporation of machine-learning schemes[13]. Although these efforts have demonstrated, to varying extents, the potential to provide insights into the physics of transport problem, they are mainly aimed at addressing the closure problem in a self-consistent, predictive manner. This highlights the strong desirability of a simulation tool based on less computationally-costly fluid descriptions (such as MICaPS), capable of resolving the anomalous electron cross-field current in a range of operating conditions and across thruster designs, even though the physics governing the observed behaviors might not be very accurately captured.

As the second point, even if the developed comprehensive model intrinsically allows assessing the influences of intensive parameters and their gradients on the unsteady plasma phenomena and averaged performance parameters of the device, the model is not meant to reveal the underlying physics of turbulence-induced transport and/or to investigate the evolution and interactions of several co-existing wave modes. As a matter of fact, the presented scheme stands out of the framework of the simulation tools specifically developed for the purposes of studying and self-consistently capturing phenomena such as self-organization, waves saturation, modes coupling and transition whose analysis necessarily requires more complex approaches such as Particle-in-Cell[14] and direct-kinetic simulations[15].

Keeping in mind the discussions above, we describe in Section II the different modules of the MICaPS, with a particular focus on the Stability Analysis Module (SAM). In Section III, we discuss the SAM's results regarding the characterization of wave modes in various regions of two Hall thrusters. In fact, the majority of the present paper is focused on this newly-developed module, its characteristics and performance. Nevertheless, some preliminary results of the MICaPS are also presented and discussed in Section III. Finally, Section IV includes a summary of the main outcomes from this work and outlines the perspective of the future activities.

II. Description of the Simulation Modules

The MICaPS consists of three inter-related modules as was shown schematically in Figure 1: **Baseline** plasma simulation code, Unified Anomalous Transport Code (**UATC**), and the Stability Analysis Module (**SAM**). The iteration scheme between these modules is defined such that the SAM and the UATC work as two connected functions embedded inside the Baseline. In this sense, as it was summarized in Figure 1, the SAM function receives the distributions of the plasma parameters at equilibrium from the Baseline and provides UATC with the characteristics of the detected unstable modes whose effects on axial electron momentum are defined in terms of closure models for different thruster regions. The UATC, in turn, provides the Baseline with the profile of the anomalous collision frequency that is then implemented in the Ohm's law and the iteration continues until convergence.

It is important to highlight that based on the mentality behind the MICaPS, as elaborated on in Section I, the closure laws in the different thruster regions have been assumed to remain unchanged. In this respect, for different operating conditions and in each specific region, the influence of changes in local plasma parameters on the instabilities' contribution to transport is reflected in the model through the change in the magnitude of the local anomalous collision frequencies obtained from the region's closure law. In other words, noting the dependency of the SAM on the local plasma parameters to predict the wave properties, and the observed sensitivity of the closure laws in UATC on the main characteristics of the waves (mode number, frequency and growth rate)[11], the significance of the anomalous collision frequency contribution to cross-field motion changes for different operating conditions as the predicted parameters of the waves vary, even if the closure laws are kept the same.

A. Baseline Plasma Simulation Module

The Baseline model is a quasi-2D fluid plasma simulation that solves the conservation equations for the electrons, ions and neutrals on a magnetic-field-aligned mesh. The main idea behind the development of this model was to obtain a simplified, though sufficiently accurate, first-order description of plasma behavior in Hall thrusters with the capability of taking into account complex 2D magnetic field topologies such as that of the magnetic shielding scheme. The model itself, together with its application to investigate magnetic field effects on a Hall thruster performance, is described in great detail in Refs. 16, 17 and 18. Figure 2 shows the Baseline simulation domain for a typical Hall thruster geometry and the magnetic coordinates λ and μ of the field-aligned mesh, defined respectively in the direction along and perpendicular to the local magnetic field vector. In addition, Figure 3 shows the results of the Baseline model in terms of the main plasma parameters, reproduced from Ref. 16. The results correspond to the simulation of the SITAEL's HT5k thruster in its nominal operating condition.

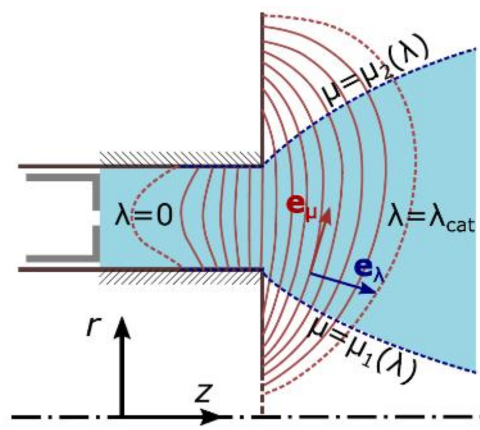

Figure 2: Baseline model simulation domain and the magnetic coordinates defined on the 2D magnetic field; reproduced from Ref. 18.

Of particular relevance to the present work, the anomalous electron transport has been introduced in the Baseline by considering a Bohm relation of the form $\upsilon_{an} = \alpha_B \omega_{ce}$, where α_B is an empirical parameter, calibrated on the thrust and current measurements, and ω_{ce} is the electron cyclotron frequency. The original Bohm turbulent-diffusion relation has been derived for turbulence-induced $\tilde{E}/B$ diffusion of particles moving at the thermal velocity with a diffusion step size on the order of Larmor radius, and under the assumption of saturated waves amplitude being on the order of electron temperature. Although this approach has been in use in various plasma simulations[19], the Bohm model does not represent a very accurate model for electron cross-field transport in Hall thrusters. This is primarily because the underlying assumptions of this relation does not strictly hold under various plasma conditions and in different regions of the thruster where the plasma properties and the wave characteristics change significantly. As a result, the need to improve the description of the anomalous mobility in the Baseline model served as the initial motive behind the development of the UATC module, as will be described in the following section.

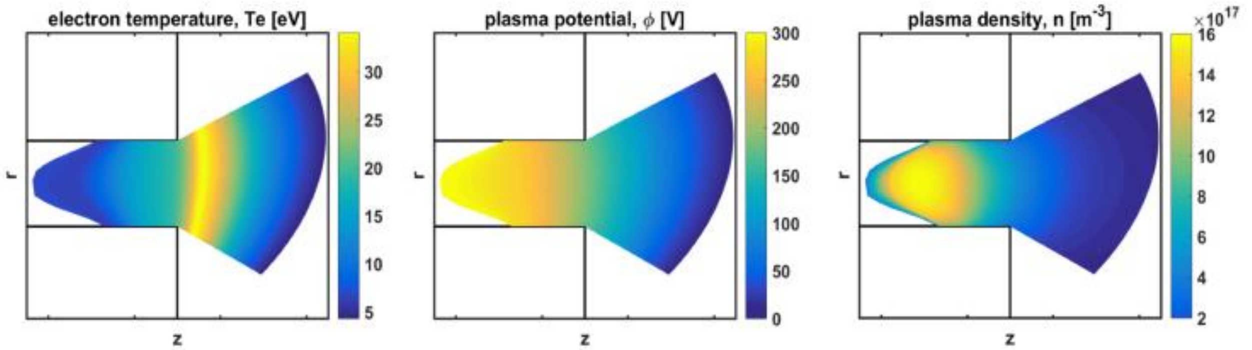

Figure 3: Simulation results of the electron temperature, plasma potential and plasma density of the HT5k; reproduced from Ref. 16.

B. Unified Anomalous Transport Module

The Unified Anomalous Transport Module provides a set of closure models for the three regions of the Hall thruster simulation domain, linking the values and the gradients of intensive plasma parameters in each region to an "anomalous" collision frequency along the centerline of the thruster discharge channel. To this end, the UATC module includes the models that capture the most relevant physics of the current-inducing instabilities considered to be dominant in different thruster's regions. In a previous work[11], we extensively discussed the physics of the considered transport mechanisms, the models that resolve the cross-field current induced by each mechanism, and preliminary results of the "Complemented" code, resulted from the implementation of the UATC into the Baseline. Figure 4 shows some of the results presented and discussed in Ref. 20, obtained from the complemented code for the HT5k thruster for the same operating condition as that corresponding to Figure 3.

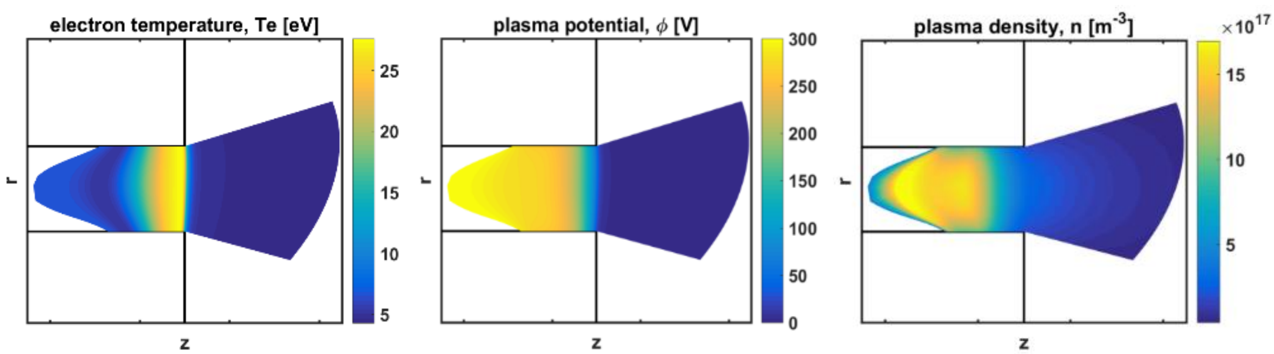

Figure 4: Simulation results of the SITAEL's HT5k Hall thruster using the Complemented code (Baseline plus UATC), reproduced from Ref. 20.

An important point to highlight is that a turbulent plasma is characterized by several co-existing wave modes, interacting with each other and with the plasma particles. As a result, the actual "turbulence-induced" electron cross-field diffusion, amounting to the estimation of turbulent scattering rate caused by all the co-existing modes, is greatly complex to accurately capture self-consistently in a fluid simulation. Consequently, a main assumption of the UATC is that in each region (for longitudinal waves), or axial location (for azimuthal waves), the fastest-growing unstable mode has the most significant contribution to cross-field transport and, thus, the induced current due to that single mode represents a reasonably-accurate approximation of the overall diffusion due to all co-existing modes.

Furthermore, although the general formulations of the UATC module has stayed the same as those presented in Ref. 20, the code has undergone a series of updates so as to, first, allow its integration as a part of the MICaPS, and second, to reflect the recent understandings on the physics of the instabilities and their contributions to transport[12,21]. Table 1 reports the main characteristics of the UATC module, including the definition of the extent of various thruster regions, and the scaling of the anomalous collision frequency with the local plasma parameters and local wave properties in each region. It is important to mention that the beginning of the ionization region, as shown in Table 1, corresponds to the location where the neutral number density is 70% of its maximum. This is because the upstream region of the ionization zone is assumed as near-anode neutrals diffusion region where the classical transport is dominant.

Table 1: Summary of the definitions and characteristics of the Unified Anomalous Transport Module; n_n and n are, respectively, the neutral density and the plasma density at equilibrium. B_r is radial component of the magnetic field vector along the channel centerline. X corresponds to the axial location at which the condition within the parentheses is met. L_c is the thruster channel length.

Region	Ionization	Acceleration	Near-Plume
Axial Extent	$\mathrm{X}\left(0.7n_{n0,max}\right) < x \leq \mathrm{X}(0.1n_{n0,max})$	$\mathrm{X}(n_{0max}) < x \leq \max\{\mathrm{X}\left(0.9B_{r,max}\right)\}$	$\mathrm{X}\left(B_{r,max}\right) < x \leq 2.5L_c$
Transport Mechanism	Rotating Spoke Instability	Beam-Plasma Instability	Electron Cyclotron Drift Instability
$\boldsymbol{v_{an}}$ **Scaling**	$\sim \frac{k^2 T_e^2 B}{E_x^2}$	$\sim \frac{1}{1 - k(\frac{m_e \langle E_x \rangle}{eB^2})}$	$\sim \exp\left(\int \frac{\alpha\sqrt{\frac{n}{c_s}}E_x}{BV_{di}}dx - \ln\left(\frac{nV_{di}}{(nV_{di})_{ref}}\right)\right)$

In Table 1, k represents the wave number of instability wave, T_e is the local electron temperature, E_x is the local axial electric field, and $\langle E_x \rangle$ in the v_{an} scaling relation for the beam-plasma instability denotes the average of equilibrium electric field over the length of the acceleration region. In addition, B is the magnetic field intensity, which, along the thruster channel centerline, is assumed to be almost equal to the magnitude of the radial component of the B vector (B_r). Finally, the parameters n, c_s and V_{di} are, respectively, the plasma density, ion sound speed and the ion beam velocity, and α is a constant.

C. Plasma Stability Analysis Module

The **S**tability **A**nalysis **M**odule (SAM) is a two-fluid (ions and electrons) simulation model that solves a linearized perturbed system of equations in the axial and azimuthal directions. A unique feature of SAM is its capability to assess the stability of both low-and high-frequency plasma wave modes in an extended domain, from inside the discharge channel into the near-plume region.

As SAM complements the UATC and the Baseline modules to form the MICaPS, it does not require to resolve the equilibrium plasma properties and their axial variations along the channel centerline, being these derived from the solution of the Baseline model. Moreover, the coupling between SAM and the Baseline allows, in particular, the investigation of the ionization-induced instabilities without the need to include the continuity and momentum equations of the neutrals in the perturbed system of equations. In fact, as also demonstrated by other authors[22,23], it is a reasonable assumption in studying these instabilities to neglect the perturbations in neutral flow velocity and in the effective ionization and electron-neutral collision rates, i.e. $\sigma_i u_e$ and $\sigma_{en} u_e$. As a result, in the SAM's formulation (see Section C.1), the effect of collisions with neutrals is introduced into the perturbed system of equations in terms of steady-state effective ionization and electron-neutral collision frequencies from the baseline. Furthermore, the velocity of the neutral flow is assumed to be constant and in the axial direction, equal to the neutral thermal injection velocity at the gas distributor temperature.

In the subsequent sections, the system of equations and the procedure followed to derive the dispersion relation and its solutions are described. The formulations for both low-frequency and high-frequency analyses are presented and the relevant assumptions are specified.

C.1. General System of Equations and the Solution Procedure

The continuity and momentum conservation equations for the electron and ion flows, as shown by Eqs. 2.1 to 2.4, form the basis of the model:

$$\frac{\partial n}{\partial t} + \vec{u}_e \cdot \nabla n = n\vartheta_i \quad (2.1)$$

$$\frac{\partial n}{\partial t} + \vec{u}_i \cdot \nabla n = n\vartheta_i \quad (2.2)$$

$$-ne(\vec{E}+\vec{u}_e\times\vec{B})-\nabla p_e-m_e n\vartheta_e\vec{u}_e=m_e n\frac{\partial\vec{u}_e}{\partial t}+\vec{u}_e\cdot\nabla\vec{u}_e \tag{2.3}$$

$$ne\vec{E}-m_i n\vartheta_i(\vec{u}_i-\vec{u}_n)=m_i n\frac{\partial\vec{u}_i}{\partial t}+\vec{u}_i\cdot\nabla\vec{u}_i \tag{2.4}$$

The above system of equations is complemented by the equation of state for electrons such that

$$\nabla p_e=T_e\nabla n \tag{2.5}$$

In the above equations, n is the plasma number density, ϑ_i and ϑ_e are the ionization and electron-neutral collision frequencies, respectively, and $\vec{u}_e$, $\vec{u}_i$ and $\vec{u}_n$ are the electron, ion and neutral flow velocities. p_e is the electron pressure which in its gradient definition, Eq. (2.5), T_e is the electron temperature in eV. It is also necessary to point out that whereas, in general, the electron temperature is retained in the formulation, it is assumed to remain unperturbed and thus, the electron energy equation is not included.

For the purpose of the stability analyses performed, quasi-neutrality is assumed for both the unperturbed and perturbed plasma number density, i.e. $n_{e0}=n_{i0}=n_0$ and $n_e'=n_i'=n'$, respectively. This assumption is supported by the fact that the Debye length is much smaller than the dimensions of the thruster, and than the characteristic length scales of the perturbations to be studied. Furthermore, the ions are considered very weakly-magnetized and thus, only the electrostatic force is retained in the ion momentum equation. Additionally, the ion-ion collisions, and therefore, the ion pressure term, is excluded from Eq. (2.4). Finally, the electron velocity is assumed to be much larger than the neutral flow velocity, and as a result, in Eq. (2.3), the $\vec{u}_n$ is neglected compared to $\vec{u}_e$ in the term corresponding to electron-neutral collisional momentum exchange (the third term on the left-hand side).

The 2D cartesian geometry of the problem is defined as follows: the x-coordinate is along the axis of the thruster discharge channel, the y-coordinate is in the direction of the normal to inner channel wall surface and the z-coordinate (azimuthal direction) completes the orthogonal right-handed coordinate system. The unperturbed component of the electric field is in the positive x direction whereas the externally-applied magnetic field vector is assumed to be radial and pointing in the negative y direction. As a result, the positive z direction indicates the direction of the $-\vec{E}\times\vec{B}$ vector. The assumption of the radial steady magnetic field vector, i.e. $\vec{B}=-B_0\hat{\jmath}$, is justified since the stability studies are performed along the channel centerline of the Hall thruster where the magnetic field lines are mostly radial.

Substituting Eq. 2.5 into the Eq. 2.3, the above system of equations is written in the component form, yielding

$$\frac{\partial n}{\partial t}+n\left(\frac{\partial u_{ex}}{\partial x}+\frac{\partial u_{ez}}{\partial z}-\vartheta_i\right)+u_{ex}\frac{\partial n}{\partial x}+u_{ez}\frac{\partial n}{\partial z}=0 \tag{2.6}$$

$$\frac{\partial n}{\partial t}+n\left(\frac{\partial u_{ix}}{\partial x}+\frac{\partial u_{iz}}{\partial z}-\vartheta_i\right)+u_{ix}\frac{\partial n}{\partial x}+u_{iz}\frac{\partial n}{\partial z}=0 \tag{2.7}$$

$$-ne\left(-\frac{\partial\varphi}{\partial x}+B_0u_{ez}\right)-T_e\frac{\partial n}{\partial x}-m_e n\vartheta_e u_{ex}=m_e n\left(u_{ex}\frac{\partial u_{ex}}{\partial x}+u_{ez}\frac{\partial u_{ex}}{\partial z}+\frac{\partial u_{ex}}{\partial t}\right) \tag{2.8}$$

$$-ne\left(-\frac{\partial\varphi}{\partial z}-B_0u_{ex}\right)-T_e\frac{\partial n}{\partial z}-m_e n\vartheta_e u_{ez}=m_e n\left(u_{ex}\frac{\partial u_{ez}}{\partial x}+u_{ez}\frac{\partial u_{ez}}{\partial z}+\frac{\partial u_{ez}}{\partial t}\right) \tag{2.9}$$

$$-ne\frac{\partial\varphi}{\partial x}-m_i n\vartheta_i(u_{ix}-u_{nx})=m_i n\left(u_{ix}\frac{\partial u_{ix}}{\partial x}+u_{iz}\frac{\partial u_{ix}}{\partial z}+\frac{\partial u_{ix}}{\partial t}\right) \tag{2.10}$$

$$-ne\frac{\partial\varphi}{\partial z}-m_i n\vartheta_i(u_{iz}-u_{nz})=m_i n\left(u_{ix}\frac{\partial u_{iz}}{\partial x}+u_{iz}\frac{\partial u_{iz}}{\partial z}+\frac{\partial u_{iz}}{\partial t}\right) \tag{2.11}$$

As it can be seen from the above equations, the implemented formulation in SAM is electrostatic. This means assuming the same direction for the wave propagation vector ($\vec{k}$) and the electric field fluctuations ($\vec{E}'$). As a result, no perturbed magnetic field component is considered, and the overall electric field vector can be expressed as $\vec{E}=-\nabla\varphi$.

The baseline model's predictions of the steady-state plasma properties along the channel centerline satisfies the following system of unperturbed equations, derived for the equations (2.6) to (2.11)

$$n_0\left(\frac{du_{e0x}}{dx} - \vartheta_i\right) + u_{e0x}\frac{dn_0}{dx} = 0 \tag{2.12}$$

$$n_0\left(\frac{du_{i0x}}{dx} - \vartheta_i\right) + u_{i0x}\frac{dn_0}{dx} = 0 \tag{2.13}$$

$$-en_0\left(-\frac{d\varphi_0}{dx} + B_0 u_{e0z}\right) - T_{e0}\frac{dn_0}{dx} - m_e n_0 \vartheta_e u_{e0x} = m_e n_0\left(u_{e0x}\frac{du_{e0x}}{dx}\right) \tag{2.14}$$

$$en_0 B_0 u_{e0x} - m_e n_0 \vartheta_e u_{e0z} = m_e n_0\left(u_{e0x}\frac{\partial u_{e0z}}{\partial x}\right) \tag{2.15}$$

$$-en_0\frac{d\varphi_0}{dx} - m_i n_0 \vartheta_i (u_{i0x} - u_{n0x}) = m_i n_0\left(u_{i0x}\frac{du_{i0x}}{dx}\right) \tag{2.16}$$

Comparing the above system with that given by Eqs. (2.6) to (2.11), it is evident that the steady-state ion velocity in the azimuthal direction is neglected. In addition, the steady-state unperturbed plasma properties are assumed to be uniform along the channel azimuthal direction.

The overall plasma parameters are substituted in Eqs. (2.6) to (2.11) using the relation given by Eq. 2.17

$$\psi(x,z,t) = \psi_0(x) + \psi'(x,z,t), \tag{2.17}$$

where ψ is either a vector or a scalar quantity. Assuming small-amplitude fluctuations with respect to steady-state values, i.e. $|\psi'| \ll |\psi_0|$, the obtained equations are linearized to derive the perturbed system of equations, Eqs. (2.18) to (2.23). Considering the perturbed terms to be harmonic and periodic in space and time, or of the form exp $[i(k_x x + k_z z - \omega t)]$, the below system of algebraic equations governs the spatial evolution of the amplitude of the fluctuating plasma parameters as implicit functions of the axial and azimuthal wave numbers (k_x and k_z) and the complex frequency (ω).

$$\left(-i\omega + ik_x u_{eox} + ik_z u_{eoz} + \frac{du_{e0x}}{dx} - v_i\right)\tilde{n} + \left(ik_x n_0 + \frac{dn_0}{dx}\right)\widetilde{u_{ex}} + (ik_z n_0)\widetilde{u_{ez}} = 0 \tag{2.18}$$

$$\left(-i\omega + \frac{du_{iox}}{dx} - v_i + ik_x u_{i0x}\right)\tilde{n} + \left(in_0 k_x + \frac{dn_0}{dx}\right)\widetilde{u_{\iota x}} + (ik_z n_0)\widetilde{u_{\iota z}} = 0 \tag{2.19}$$

$$\begin{aligned}&\left(m_e u_{e0x}\frac{du_{e0n}}{dx} - e\frac{d\varphi_0}{dx} + eB_0 u_{e0z} + ik_x T_e + m_e v_e u_{e0x}\right)\tilde{n}\\ &\quad + \left(-i\omega m_e n_0 + ik_x m_e n_0 u_{e0x} + m_e n_0\frac{du_{e0x}}{dx} + ik_z m_e n_0 u_{e0z} + m_e n_0 v_e\right)\widetilde{u_{ex}}\\ &\quad + (n_0 B_0)\widetilde{u_{ez}} + (-ien_0 k_x)\tilde{\varphi} = 0\end{aligned} \tag{2.20}$$

$$\begin{aligned}&\left(m_e u_{e0x}\frac{du_{e0z}}{dx} + m_e v_e u_{e0z} + ik_z T_e - eB_0 u_{e0x}\right)\tilde{n} + \left(m_e n_0\frac{du_{e0x}}{dx} - en_0 B_0\right)\widetilde{u_{ex}}\\ &\quad + (-i\omega m_e n_0 + ik_x m_e n_0 u_{e0x} + ik_z m_e n u_{e0z} + m_e n_0 v_e)\widetilde{u_{ez}} + (-ik_z e n_0)\tilde{\varphi} = 0\end{aligned} \tag{2.21}$$

$$\begin{aligned}&\left(-e\frac{d\varphi_0}{dx} - m_i v_i (u_{i0x} - u_{n0x}) - m_i u_{i0x}\frac{du_{i0x}}{dx}\right)\tilde{n}\\ &\quad + \left(i\omega n_0 m_i - m_i n_0 v_i - im_i n_0 k_x u_{i0x} - m_i n_0\frac{du_{i0x}}{dx}\right)\widetilde{u_{\iota x}} + (-ien_0 k_x)\tilde{\varphi} = 0\end{aligned} \tag{2.22}$$

$$(i\omega n_0 m_i - m_i n_0 v_i - ik_x m_i n_0 u_{i0x})\widetilde{u_{\iota z}} + (-ien_0 k_z)\tilde{\varphi} = 0 \tag{2.23}$$

The above equations are in the most general form, including all relevant terms. However, considering the time scales of a problem at hand, simplifying assumptions can be introduced to obtain two subsets of the governing equations, one for the low-frequency and the other for the high-frequency range. These two subsets are presented separately in the subsequent sections. Nevertheless, in both cases, the system of perturbed linearized algebraic equations is written in the general matrix form, Eq. (2.24), and translates into an eigenvalue problem for the unknown complex frequency $\omega = \omega_r + i\omega_i$.

$$A\widetilde{\boldsymbol{P}} = 0 \tag{2.24}$$

In Eq. (2.24), $\widetilde{\boldsymbol{P}}$ is a vector whose components are the fluctuation amplitudes of the plasma parameters, $\widetilde{\boldsymbol{P}} = [\tilde{n}, \widetilde{u_{ex}}, \widetilde{u_{ez}}, \widetilde{u_{ix}}, \widetilde{u_{iz}}, \tilde{\varphi}]$. A is the matrix of coefficients whose determinant gives the dispersion relation of the electrostatic waves. The dispersion relation is then solved for the complex ω, assigning values to k_x and k_z depending on the wave propagation direction of interest and the range of wavelengths to be investigated. Among the solutions of the dispersion relation, those with positive imaginary part of the frequency ($\omega_i > 0$) are unstable and their growth rate (γ) is equal to ω_i. The solution process is carried out at each axial location within a specific region. It is important to note that based on the formulation presented above and as it will be seen in the two following sections, the dispersion relation is at least of the third order in ω, which implies at least three possible solutions at each axial position and for each pair of (k_x, k_z). As a result, among these solutions, to select a dominant unstable wave mode at each axial location, the following criteria were taken into account:

1. **Low-Frequency wave modes**: 5 kHz $\leq \omega_r \leq$ 100 kHz, and max ($0 < \omega_i <$ 500 kHz),
2. **High-Frequency wave modes**: 500 kHz $\leq \omega_r \leq$ 20 MHz, and max ($0 < \omega_i <$ 500 kHz).

The above ranges for the real frequency component were considered as the selection criteria since in the present effort, we are interested in investigating the presence and characteristics of the rotating spoke instability in the low-frequency range, and the beam-plasma instability in the high-frequency range.

C.2. System of Equation for Low-Frequency Analysis

In the low-frequency range, it is reasonable to neglect the electron inertia terms, i.e. the right-hand side of the Eqs. (2.8) and (2.9). This is because the time scale of the oscillations is much smaller than the characteristic time of the electron thermal and cyclotron motions, i.e. $\omega \ll \omega_{pe}, \omega_{ce}$, where ω_{pe} and ω_{ce} are the electron plasma and cyclotron frequencies. Moreover, to further simplify the system and to obtain a formulation that is more robust to solve numerically, the terms corresponding to the derivatives of the unperturbed plasma parameters have been substituted for using the steady-state equations, Eq. (2.12) to (2.16) with the electron inertia terms neglected. Finally, the equations were normalized using appropriate reference values.

As a result of the aforementioned manipulations of the equations, the matrix of coefficients A can be written as in Eq. (2.25) in terms of the normalized parameters of the general form χ^*

$$A = \begin{pmatrix} -i\omega^* + (ik_x^*+1)u_{e0x}^* + ik_z^* u_{e0z}^* & ik_x^*-1 & ik_z^* & 0 & 0 & 0 \\ -i\omega^* + (ik_x^*+1)u_{i0x}^* & 0 & 0 & ik_x^*-1 & ik_z^* & 0 \\ (u_{e0z}^* - v_i^* u_{n0x}^* - u_{i0x}^*)(ik_x^*+1) & HP & 1 & 0 & 0 & -ik_x^* \\ ik_z^*(u_{e0z}^* - v_i^* u_{n0x}^* - u_{i0x}^*) & -1 & HP & 0 & 0 & -ik_z^* \\ 0 & 0 & 0 & -i\omega^* - (ik_x^*+1)u_{i0x}^* & 0 & -ik_x^* \\ 0 & 0 & 0 & 0 & i\omega^* - ik_x^* u_{i0x}^* - v_i^* & -ik_z^* \end{pmatrix}. \tag{2.25}$$

The term HP in the matrix A denotes the inverse of the Hall parameter, or v_{en0}/ω_{ce}.

In addition, since the electron inertia terms and electromagnetic effects are neglected in the formulation, the components of matrix A corresponding to $\widetilde{u_{ex}}^*$, $\widetilde{u_{ez}}^*$ and $\tilde{\varphi}^*$ of the normalized vector of unknowns $\widetilde{\boldsymbol{P}}^*$ do not contribute to the order of the dispersion relation and thus, the possible solutions for the complex frequency ω. Therefore, following the Gaussian elimination approach, these unknowns can be substituted for, resulting in a reduced-order 3-by-3 matrix A', whose determinant gives the characteristic equation. This equation is solved in the way described in Section C.1.

C.3. System of Equation for High-Frequency Analysis

To assess the stability of wave modes in the high-frequency range, the electron inertia terms are retained in the formulation whereas the pressure gradient term in the electron momentum equations, (2.20) and (2.21), is neglected. As a result, the following system of equations is obtained:

$$(-i\omega + ik_x u_{e0x} + ik_z u_{e0z} + \frac{du_{e0x}}{dx} - v_i)\tilde{n} + \left(ik_x n_0 + \frac{dn_0}{dx}\right)\widetilde{u_{ex}} + (ik_z n_0)\widetilde{u_{ez}} = 0 \tag{2.26}$$

$$\left(-i\omega + \frac{du_{i0x}}{dx} - v_i + ik_x u_{i0x}\right)\tilde{n} + \left(in_0 k_x + \frac{dn_0}{dx}\right)\widetilde{u_{ix}} + (ik_z n_0)\widetilde{u_{iz}} = 0 \tag{2.27}$$

$$\begin{aligned}&\left(m_e u_{eox}\frac{du_{e0n}}{dx} - e\frac{d\varphi_0}{dx} + eB_0 u_{e0z} + m_e v_e u_{e0x}\right)\tilde{n}\\ &\qquad + \left(-i\omega m_e n_0 + ik_x m_e n_0 u_{e0x} + m_e n_0\frac{du_{e0x}}{dx} + ik_z m_e n_0 u_{e0z} + m_e n_0 v_e\right)\widetilde{u_{ex}}\\ &\qquad + (n_0 B_0)\widetilde{u_{ez}} + (-ien_0 k_x)\tilde{\varphi} = 0\end{aligned} \tag{2.28}$$

$$\begin{aligned}&\left(m_e u_{e0x}\frac{du_{eoz}}{dx} + m_e v_e u_{e0z} - eB_0 u_{e0x}\right)\tilde{n} + \left(m_e n_0\frac{du_{eox}}{dx} - en_0 B_0\right)\widetilde{u_{ex}}\\ &\qquad + (-i\omega m_e n_0 + ik_x m_e n_0 u_{e0x} + ik_z m_e n u_{e0z} + m_e n_0 v_e)\widetilde{u_{ez}} + (-ik_z e n_0)\tilde{\varphi} = 0\end{aligned} \tag{2.29}$$

$$\begin{aligned}&\left(-e\frac{d\phi_0}{dx} - m_i v_i(u_{iox} - u_{nox}) - m_i u_{iox}\frac{du_{iox}}{dx}\right)\tilde{n}\\ &\qquad + \left(i\omega n_0 m_i - m_i n_0 v_i - im_i n_0 k_x u_{i0x} - m_i n_0\frac{du_{iox}}{dx}\right)\widetilde{u_{ix}} + (-ien_0 k_x)\tilde{\varphi} = 0\end{aligned} \tag{2.30}$$

$$(i\omega n_0 m_i - m_i n_0 v_i - ik_x m_i n_0 u_{i0x})\widetilde{u_{iz}} + (-ien_0 k_z)\tilde{\varphi} = 0 \tag{2.31}$$

To obtain the matrix of coefficients A, the same approach as that for the low-frequency case were followed. Furthermore, apart from the assumption of neglecting the electron pressure gradient, other assumptions are the same as those already mentioned up to this point. In the HF range, the matrix A is of the sixth-order. Here, it is only possible to Gaussian-eliminate the components of matrix A corresponding to $\tilde{\varphi}^*$ from the system of equations. This possibility is because the formulation is still electrostatic. Thus, the reduced-order matrix of coefficients, A', is of the fifth-order and is written as

$$A' = \begin{pmatrix} a_1 & b_1 & c_1 & 0 & 0 \\ a_2 & 0 & 0 & d_2 & e_2 \\ 0 & b_3 & c_3 & 0 & e_3 \\ 0 & b_4 & c_4 & 0 & e_4 \\ 0 & 0 & 0 & d_5 & e_5 \end{pmatrix}, \tag{2.32}$$

in which, the non-zero components are

$a_1 = -i\omega^* + (ik_x^* + 1)u_{e0x}^* + ik_z^* u_{e0z}^*,$

$b_1 = ik_x^* - 1,$

$c_1 = ik_z^*,$

$a_2 = -i\omega^* + (ik_x^* + 1)u_{i0x}^*,$

$d_2 = ik_x^* - 1,$

$e_2 = ik_z^*,$

$b_3 = -i\omega^*\frac{\Omega_{ci}}{\Omega_{ce}} + ik_x^* u_{e0x}^*\frac{\Omega_{ci}}{\Omega_{ce}} - \frac{{u_{i0x}^*}^2}{u_{e0x}^*} + \frac{u_{n0x}^*}{u_{e0x}^*}v_i^*\frac{\Omega_{ci}}{B_0} - \frac{u_{e0z}^*}{u_{e0x}^*} + ik_z^* u_{e0z}^*\frac{\Omega_{ci}}{\Omega_{ce}},$

$c_3 = 1,$

$e_3 = e_5 = -\frac{k_x^*}{k_z^*}(i\omega^* - ik_x^* u_{i0x}^* - v_i^*),$

$b_4 = -\frac{\Omega_{ci}}{\Omega_{ce}}v_e^*\frac{u_{e0z}^*}{u_{e0x}^*},$

$$C_4 = \frac{\Omega_{ci}}{\Omega_{ce}}(-i\omega^* + ik_x^* u_{e0x}^* + ik_z^* u_{e0z}^* + \nu_e^*),$$

$$e_4 = -(i\omega^* - ik_x^* u_{i0x}^* - \nu_i^*),$$

$$d_5 = i\omega^* - u_{i0x}^*(ik_x^* + 1).$$

The process of solving the characteristic equation of matrix A' remains the same as that carried out to characterize the LF unstable wave modes.

III. Results and Discussion

As mentioned earlier, this paper mostly focuses on the Stability Analysis Module of the MICaPS. Thus, this section is largely dedicated to presenting and discussing the SAM predictions of the unstable modes. In any case, preliminary results of MICaPS are also presented. In particular, noting that few assumptions were introduced in the UATC simulation concerning the physical characteristics of the incorporated instabilities[20], the MICaPS results are primarily intended to demonstrate the extent of validity of these assumptions.

SAM has been applied to study the stability of the plasma discharge in two Hall thrusters, SITAEL's HT5k and the HT5k-M. The HT5k is an SPT-type 5 kW-class Hall thruster with a conventional magnetic field topology. The HT5k-M is a 5 kW-class prototype Hall thruster with a flexible magnetic circuit design that allows the thruster characterization within an almost continuous spectrum of magnetic field topologies, from the conventional unshielded to that corresponding to the magnetic-shielding scheme. More details on the two thrusters can be found in Refs. 22 and 23. As it regards the HT5k-M, this paper presents the results of stability analysis for the HT5k-M1 configuration. The M1 model differs from the HT5k thruster primarily in terms of the channel geometry. The M1 channel length is about 30% shorter than the HT5k channel and it features a chamfered exit region, representative of the end-of-life condition of the channel. Figure 5 compares the channel geometry near the exit, and the magnetic field topology in the exit and near-plume regions of the HT5k (Figure 5 (a)) and HT5k-M1 (Figure 5 (b)).

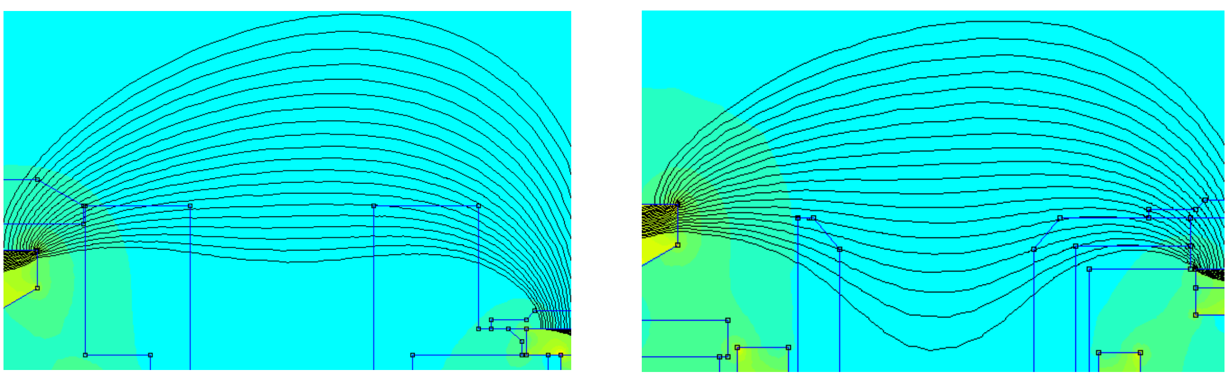

(a) (b)

Figure 5: Magnetic field topology and the channel geometry of (a) the HT5k, and (b) the HT5k-M1.

In any case, looking at the magnetic field topologies in Figure 5, it is clear that as a result of change in the channel geometry from HT5k to M1, the field topology is also, to some extent, altered. In fact, the HT5k-M1 has the so-called "lensing" characteristic over a larger extent of the discharge channel. This characteristic results in the self-consistent accelerating electric field to have a radial component, causing the ion beam to be more focused towards the centerline.

To investigate the variations in the characteristics of the unstable modes due to the change in the channel geometry and the field topology, SAM's input data from the baseline correspond to the same operating condition of the HT5k and HT5k-M1 thrusters (Table 2). Furthermore, the extent of various regions in the two thrusters are shown in Table 3, which are obtained according to the definition presented in Table 1.

Table 2: The operating condition of the HT5k and the HT5k-M1 thrusters selected for the stability analyses.

Discharge Power [kW]	Discharge voltage [V]	Magnetic field peak intensity on the channel centerline [mT]
4.5	300	20

Table 3: Description of the various regions; the extent of each region is normalized with the channel length (L) of the HT5k-M1 thruster, respectively. The HT5k channel exit plane is at 1.4L.

Hall thruster model	Ionization	Acceleration	Near-plume
HT5k	∽ 0.25L - ∽ 0.8L	∽ 0.8L - ∽ 1.6L	∽ 1.5L - 2L
HT5k-M1	∽ 0.25L - ∽ 0.7L	∽ 0.7L - ∽ 1.5L	∽ 1.4L - 2L

As it can be seen from Table 3, the change in channel geometry, and consequently, the field topology from the HT5k to HT5k-M1 results in changing of the extent and location of different regions. As it is shown in Figure 6 for the plasma density distribution (reproduced from Ref. 18), these changes cause, in general, variations in the profiles of all plasma parameters, and thus, different turbulent nature of the plasma is expected between the HT5k and the HT5k-M1. In fact, studying the stability of plasma in these two thruster configurations, interesting changes in the characteristics of the unstable modes were found which are presented in the subsequent sections.

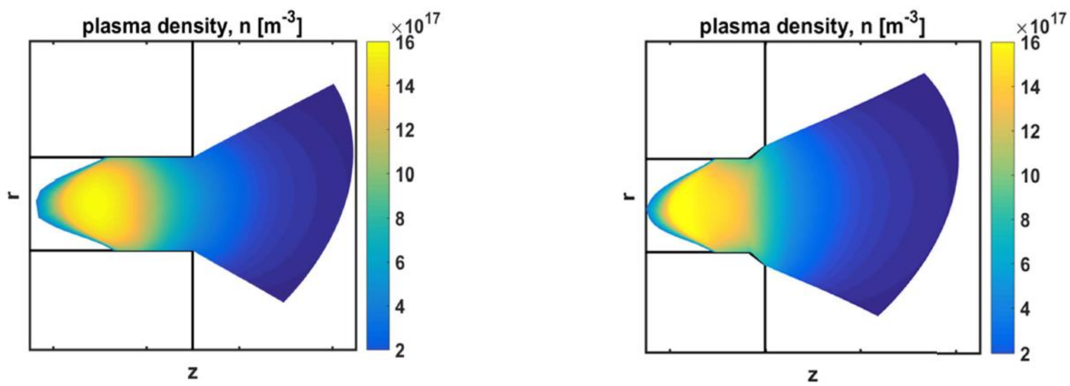

(a) (b)

Figure 6: Distribution of the plasma number density in (a) the HT5k, and (b) the HT5k-M1, reproduced from Ref. 18.

Before proceeding further, it is also important to elaborate on one point concerning the SAM formulation and its applicability. As a matter of fact, it is, first, reminded that since the electrons mobility along the magnetic field lines is significantly larger than that across the lines, the distribution of the electron temperature and plasma number density along the magnetic lines can be considered as uniform. Now, referring to Figure 5(a) and (b), in HT5k, the magnetic lines are almost radial from the inner wall to the outer whereas in the HT5k-M1, the magnetic flux parallel to the channel walls is larger. Therefore, along the radial coordinate in the HT5k-M1, the plasma parameters exhibit notable gradients. The existence of radial gradients of the plasma parameters in the HT5k-M1 implies that the results of our stability analysis, under the current formulation, are mainly valid along the channel centerline ($r = 0$) of the M1. In fact, for an appropriately-designed magnetic field topology of a Hall thruster, at the centerline along each magnetic field line, it is reasonable to assume that the plasma parameters almost reach their maximum values, thus, the radial gradients of the unperturbed plasma parameters are much smaller than the axial gradients and they can be therefore neglected.

However, in case of the HT5k (Figure 5(a)), the almost radial distribution of magnetic lines implies that the unperturbed plasma properties are almost radially constant. This means that the SAM results can be considered approximately valid also at non-zero radial locations.

The adoption of the above approach, i.e. characterizing the plasma instabilities along the channel centerline for both thrusters, roots primarily in the coupling established between the SAM and the UATC modules, recalling that the UATC currently predicts the profile of the instability-induced collision frequency along the centerline of the channel.

It is also worth mentioning that in the subsequent sections, the SAM is first used to predict the unstable modes in the HT5k and HT5k-M1 thrusters using the input data from the baseline code alone, which are obtained using an ad-hoc tunable parameter, and the Bohm turbulent diffusion description to account for the anomalous transport. However, in Section C, the SAM results using the plasma parameter profiles from the Complemented Code are reported. These input data are derived after the incorporation of the UATC in the baseline, i.e. using the instability-induced collision frequency profile along the channel centerline.

A. Unstable Wave Modes in the Ionization Region

In the ionization region, the presence of the low-frequency spoke instability has been reported by several authors in unshielded Hall thrusters[8,24,25]. The rotating spoke is an electrostatic macroscopic instability of relatively low frequency, mostly in the range of 5-25 kHz[24]. It appears as azimuthal fluctuations in electron number density and plasma potential propagating mainly in the $E \times B$ direction, with a phase velocity of about an order of magnitude lower than the electron $E \times B$ drift. The density oscillations were observed to be phase-correlated with the fluctuating electric field and, hence, this indicates the possibility of spoke's role in enhanced electron axial mobility[26].

The propagation of the instability, however, has been observed as not being purely azimuthal, but with a tilt angle of about 15-25 degrees with respect to the azimuthal plane (i.e., with a non-zero axial component of the phase velocity)[24]. Various observations in unshielded annular Hall thrusters with power levels on the order of 5-6 kW have detected the dominant spoke mode numbers (m) to be in the range of 3-6 in different operating conditions[24,27]. The wave number 'k' corresponding to the mode number 'm' is $k = m/R_c$, in which R_c is the mid-radius of the thruster channel.

With this overview of the spoke instability characteristics, in the two subsequent sections, we will present and discuss the SAM's results related to the properties of the spoke instability in the HT5k and HT5k-M1.

A.1. HT5k Thruster

Performing the stability analysis in the ionization region of the HT5k, the results show the existence of azimuthal, low-frequency unstable wave modes, propagating in the $+E \times B$ direction along the channel azimuth, with phase velocities in the range of about 1-4 km/s. As it is shown in Figure 7, different low-frequency modes excite at different axial locations along the channel centerline. The waves have frequencies from about 5 to 9 kHz and growth rates ranging from 20 to 100 kHz. Accordingly, based on the description provided above on the characteristics of the spoke, the predicted modes correspond to this instability. In addition, the stability results demonstrate that changes in the local plasma parameters in the axial direction give rise to different modes of the spoke instability to be dominant, ranging from m = 1 to m = 8. The SAM's predictions of the spoke characteristics are largely consistent with the results in Ref. 32 regarding the low-frequency ionization instabilities in an unshielded Hall thruster.

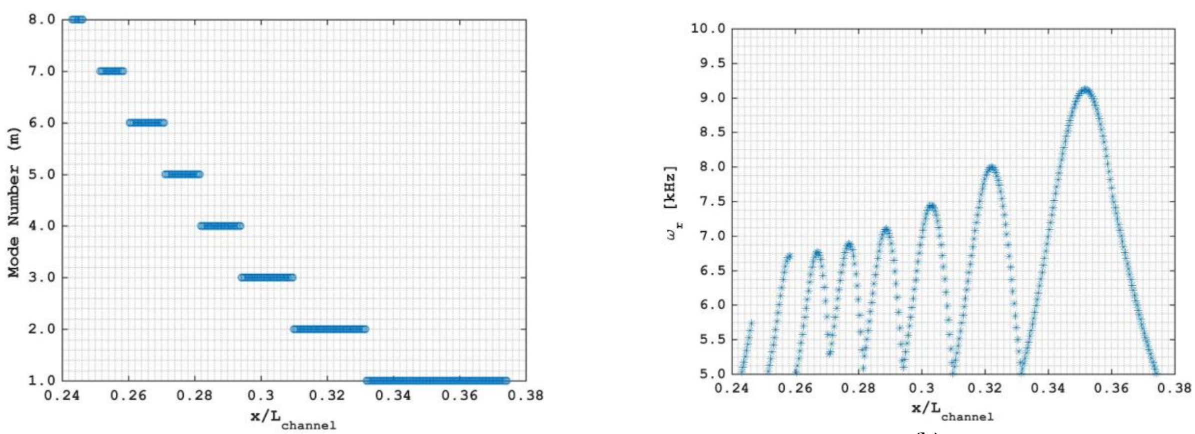

(a) (b)

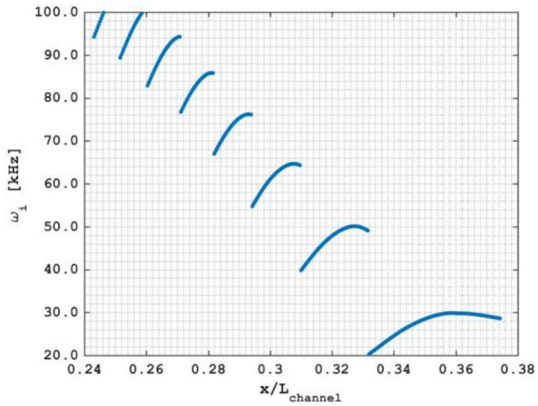

(c)

Figure 7: Characteristics of the predicted spoke modes in the ionization region of the HT5k, (a) mode number along the x-direction, (b) ω_r along x-direction, (c) ω_i along x-direction. The $L_{channel}$ corresponds to the channel length of the HT5k-M1.

It is interesting to also point out that the spoke unstable modes are only found up to about the middle of the ionization region, as defined in Table 3. Recalling the selection criteria that was implemented to choose the spoke modes among all possible solutions of the dispersion relation at each x-value, it should be noted that other unstable modes have been actually predicted for axial locations up to the end of the ionization zone. Nevertheless, the characteristics of these modes in terms of the real and/or imaginary frequencies were out of the range of values reported in literature for the spokes, and thus, we did not report those modes in the current paper. In any case, within the MICaPS framework, an assumption made is that even though the unstable modes after some axial location might not strictly correspond to "spokes" as observed numerically or experimentally, if necessary, the same anomalous transport theory of the spokes can be used to derive the axial electron current induced by these "divergent" modes.

Finally, the characteristics of the unstable waves in Figure 7 correspond to waves propagating almost-purely in the azimuthal direction, i.e. $k_z \gg k_x$. However, the spoke modes are observed to typically propagate at an angle with respect to azimuthal plane. As a result, the effects of the propagation angle ($\theta = \tan^{-1}(k_x/k_z)$) on the characteristics of the unstable modes are of interest to be studied. Nevertheless, in the context of the SAM coupling to the UATC, since at present, the theory for the spoke-induced axial electron current assumes the instability's contribution to be due to purely-azimuthal modes, the investigation of the effect(s) of tilt angle on spoke characteristics are postponed to future improvements of SAM.

A.2. HT5k-M1 Thruster

Similar to the case of HT5k, SAM predicts the excitation of spoke modes in the ionization region of the HT5k-M1. The instability waves still propagate in the $+E \times B$ direction. In addition, proceeding towards the end of the ionization zone, the mode number of the fastest-growing unstable wave decreases as was the case for the HT5k. Furthermore, the spoke modes, as selected by the criteria in Section C.1, are again found up to about half of the ionization region.

Several differences are also evident between the characteristics of the spoke in the HT5k and HT5k-M1. In particular, only the spoke modes of m = 1 and m = 2 are found to be dominant in the M1 ionization region. Noting that the channel mid-radius is the same for both thrusters, the fact that the fastest-growing modes in M1 are of lower mode numbers implies that the dominant spoke modes in M1 are of longer wavelengths compared to those in HT5k, except for the unstable waves in the axial extent of 0.33 to $0.37L_{channel}$. Furthermore, among the two dominant modes in M1 thruster, the waves corresponding to m = 2 are only dominant for a small extent in the beginning of the ionization region whereas the waves corresponding to m of 1 are dominant in most of the ionization zone.

Moreover, the frequencies of the detected spoke modes are in the range of 7-17 kHz and the growth rates are from about 40 to 100 kHz. The phase velocity of the waves encompasses a broader range with respect to that in HT5k, i.e. from 1-7 km/s. Highest phase velocities correspond to the waves with the mode number m = 1.

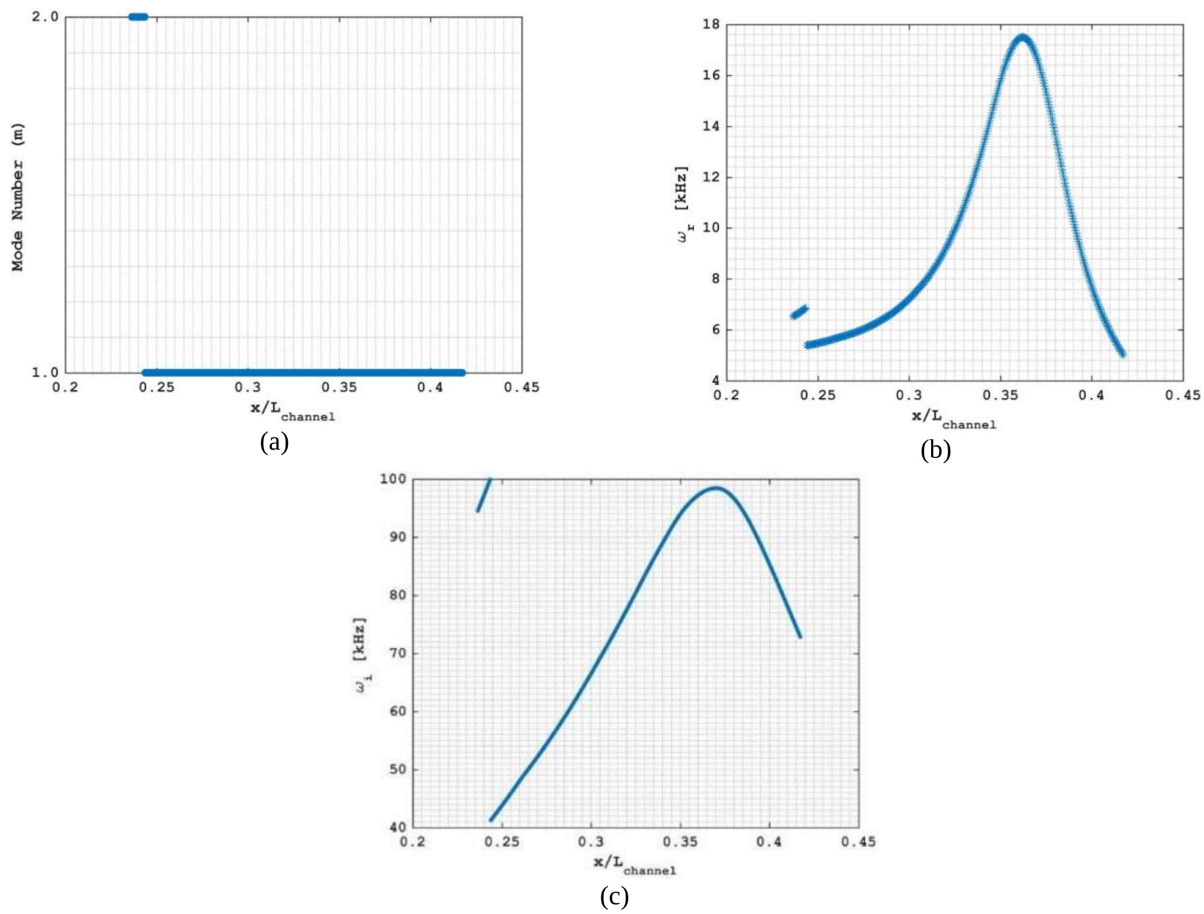

Figure 8: Characteristics of the predicted spoke modes in the ionization region of the HT5k-M1, (a) mode number along the x-direction, (b) ω_r along x-direction, (c) ω_i along x-direction. The $L_{channel}$ corresponds to the channel length of the HT5k-M1.

B. Unstable Wave Modes in the Acceleration Region

In the acceleration region of unshielded Hall thrusters, several numerical and experimental efforts have shown the beam-plasma instability to exist in the high-frequency range, and to have a considerable effect on electrons' cross-field transport[9,28]. As a result, we performed SAM simulations in the acceleration region of the HT5k and HT5k-M1 to assess primarily the existence and characteristics of this instability. This fact is also reflected in the selection criteria description in Section C.1.

To provide a brief overview, the beam-plasma instability is a high-frequency (about 2-5 MHz) axially-propagating longitudinal instability. This instability belongs to the general category of two-stream instabilities and thus, one of its excitation criteria is the existence of a sufficiently large relative drift between electrons and ion beam, which is met in the acceleration region of Hall thrusters. In fact, the reduced axial mobility (and hence, lower velocity) of electrons in Hall devices together with the presence of a high-speed ion beam can result in a two-hump distribution function of the plasma, which can give rise to the beam-plasma instability. The excitation of beam-plasma instability can be also due to Secondary Electron Emission from the channel walls. In this case, the SEE is required to reach the level corresponding to the space-charge saturated sheath[7]. Additionally, Thomas and Cappelli suggested that the beam-plasma instability can be considered as a high-frequency manifestation of the general transit-time instabilities[9].

Before moving on, it is also important to make a clarification on the extent of validity of the current stability analysis as it regards the axial instabilities in the acceleration region. As already discussed in Section C, the plasma stability formulation, at this point, resembles that of the "local" analysis. The local stability studies are considered as more accurate for investigating the plasma stability in the azimuthal direction. In applying such a study approach to the axial instabilities, we have assumed that at each axial location, an infinite, homogenous plasma with the local plasma parameters of that location exists. This implies that the interactions among various wave modes and the possible effects of the axial and radial boundaries have not been considered. As a currently-ongoing activity, the assumption of harmonic wave behaviors, i.e. enforcing fluctuations of the form exp $[i(\vec{k}\cdot\vec{x})]$, is relaxed and the axial distribution of the perturbed parameters would be solved for. This provides a more consistent description for the axial unstable modes.

Nevertheless, the idea behind adopting the local analysis approach also for the axial waves is related to description of the instability-induced axial electron current due to beam-plasma waves included in the UATC module. As a matter of fact, the theory currently assumes that as a single mode (one with the largest growth rate along the axis) of the beam-plasma excites, its fluctuating electric field at saturation contributes to electrons axial mobility through the ovalization of the particles gyro-orbits, a process sometimes referred to as "neoclassical" transport. Accordingly, by performing axial stability analysis, the primary intention is to identify such an unstable mode.

B.1. HT5k Thruster

Figure 9 shows the characteristics of the predicted axial unstable waves in the acceleration region of the HT5k. First of all, the predicted dominant modes have the wave number (k) of either -100 or -500 m^{-1}, with low wave-number modes occurring over a major part of the acceleration region. The wave number of the modes are consistent with those reported in Ref. 9 through direct solution of the dispersion relation of the transit-time instabilities[29,30]. In addition, similar to the results in Ref. 9, the phase velocities are on the same order of magnitude of the local ion beam velocity.

However, whereas the modes with k =-500 m^{-1} have real frequencies comparable with those of the beam-plasma, as reported by Thomas and Cappelli[9], the low wave-number modes (k = -100 m^{-1}) have frequencies about an order of magnitude lower, and from the real frequency perspective, are more consistent with the transit-time waves. In this respect, however, the propagation direction of the predicted modes (determined from the sign of the k) are towards the anode whereas transit-time waves are known to propagate towards the plume[1,29].

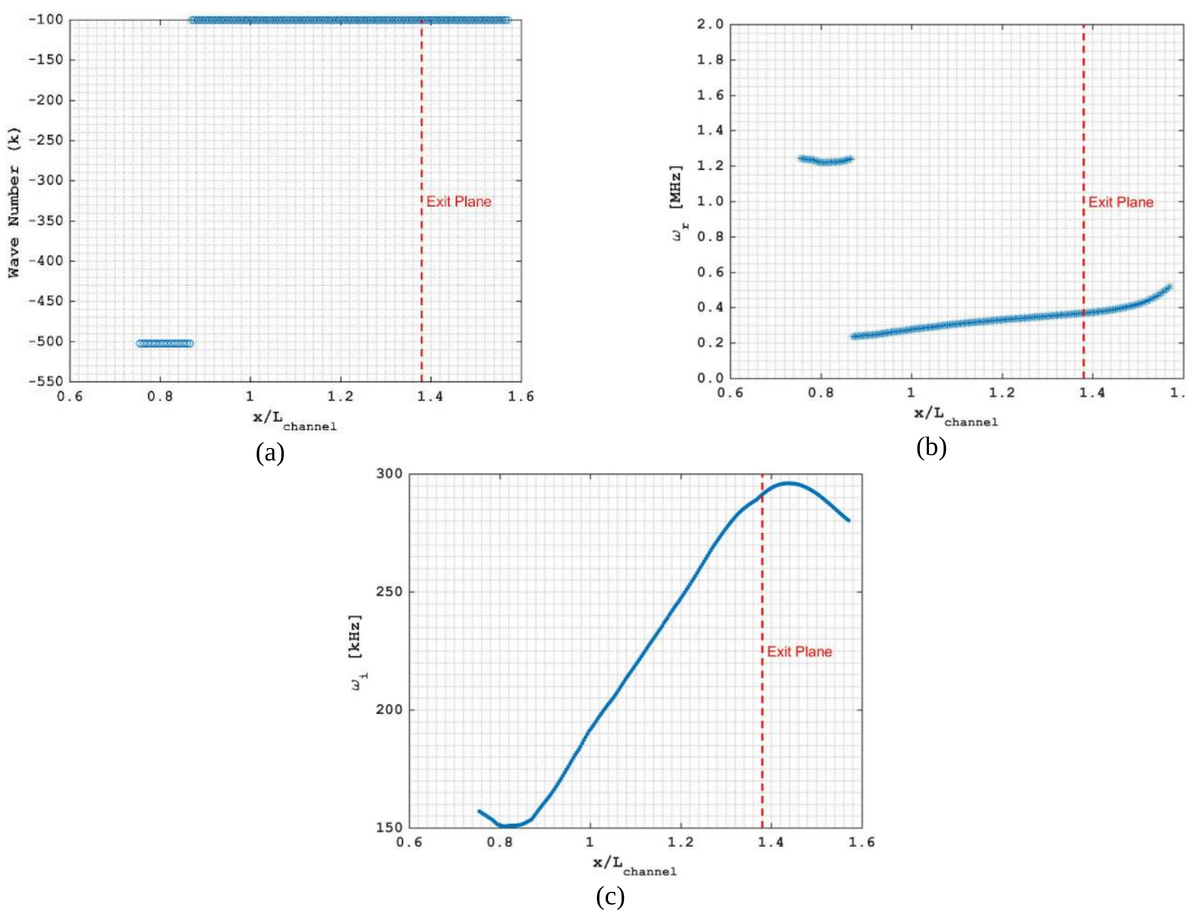

Figure 9: Characteristics of the axial high-frequency modes in the acceleration region of the HT5k, (a) wave number along the x-direction, (b) ω_r along x-direction, (c) ω_i along x-direction. The $L_{channel}$ corresponds to the channel length of the HT5k-M1.

The reason for the somewhat "peculiar" characteristics of the axial modes predicted by SAM can be associated with the adoption of the local stability analysis approach. Ongoing SAM upgrades, as described in the previous section, allow investigating the validity of this conjecture. Nevertheless, recalling the basis of the theory taken into account for the anomalous electron transport in the acceleration region, the current results on the wave properties do not undermine the UATC-SAM coupling.

B.2. HT5k-M1 Thruster

Like the unstable axial modes in the HT5k, the predicted waves in the HT5k-M1 also have the wave numbers of either -100 or -500 m^{-1}. However, the wave modes inside the channel, and close to the exit plane, with k = -100 m^{-1} are the only modes that similar to the case of HT5k, resemble the transit-time instability waves. Other waves have all real frequencies in the range of 1.5 to about 5 MHz, consistent with the characteristics of the beam-plasma waves obtained in Ref. 9.

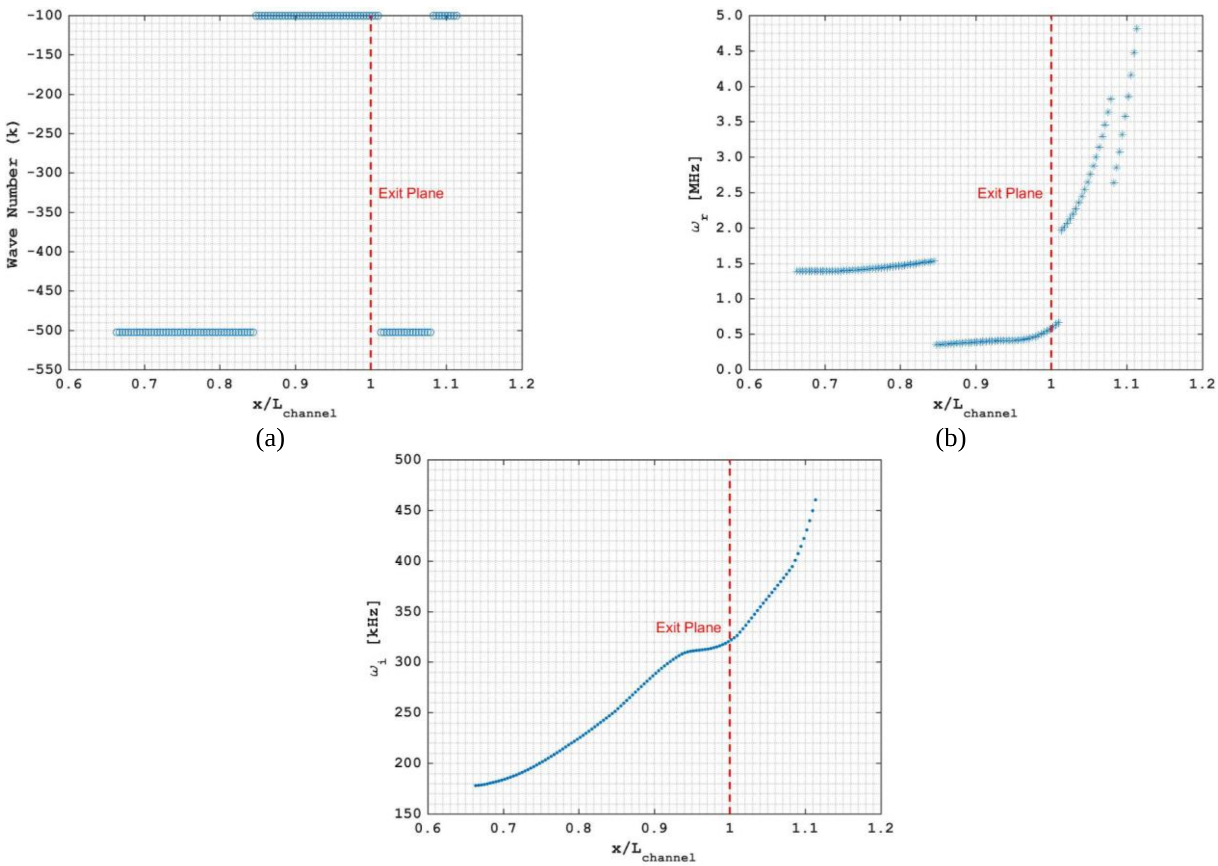

(c)

Figure 10: Characteristics of the axial high-frequency modes in the acceleration region of the HT5k-M1, (a) wave number along the x-direction, (b) ω_r along x-direction, (c) ω_i along x-direction. The $L_{channel}$ corresponds to the channel length of the HT5k-M1.

As a result, except for the modes predicted within the range of about 0.85L to 1.0L, the others can be categorized as beam-plasma instability modes with high certainty. For the case of M1, the waves phase velocities are in very good quantitative agreement with the local ion beam velocity.

Furthermore, looking at Figure 10(b) and (c), for the modes beyond the exit plane, both real and imaginary parts of the frequency are coherently increasing. This result is also consistent with the beam-plasma wave properties, reported in ref. 31, which were obtained using a hybrid/PIC simulation in the 2D r-z coordinates.

C. Comparison of the Plasma Stability in the HT5k vs. HT5k-M1 Configurations

In this section, we provide a comparative analysis of the plasma stability in the two thruster configurations in terms of the characteristics of the spoke and high-frequency axial modes detected. Figure 11 shows the comparisons between the mode number, frequency and growth rate of the spoke modes in the HT5k and HT5k-M1. In addition, Figure 12 presents the comparisons in terms of the same parameters between the two thrusters but for the high-frequency modes.

Referring to Figure 11 and Figure 12, it can be observed that, as asserted in the beginning of this section, the change in plasma properties changes the turbulent nature of the plasma. In fact, as shown in Figure 11(a), the spoke modes in HT5k-

M1 start to become unstable closer to the anode, and have only two dominant modes of m = 1 and 2. Moreover, the unstable m = 1 modes persist over a much broader extent of the ionization zone than that in HT5k. This means that in the M1 configuration and in the range of 0.24L-0.42L, the m = 1 mode has consistently larger growth rates than the modes with other m values.

Besides, as it can be seen from Figure 11(b) and (c), for both the HT5k and HT5k-M1, towards the end of the ionization region, the frequency and growth rate of the m = 1 spoke mode first increases and then decreases. Nevertheless, the growth rate and frequency of this mode in M1 thruster reaches peak values much larger than those for the m = 1 mode in HT5k.

As it concerns the contribution of unstable spoke modes to cross-field transport, the HT5k may exhibit higher discharge currents than the M1 in the same operating condition. This is because, first, waves with higher mode numbers excite in HT5k, meaning that more local zones of enhanced axial current conduction due to azimuthal perturbed electric field exist. Second, the modes with large mode numbers (m = 4 to 8) also show larger growth rates in HT5k compared to m=1 mode in M1 over the same axial extent. This implies that for a same initial wave amplitude and over an equal time interval within a current oscillation period, the spoke modes in HT5k have larger amplitudes compared to those in M1, thus, causing larger instability-induced axial currents.

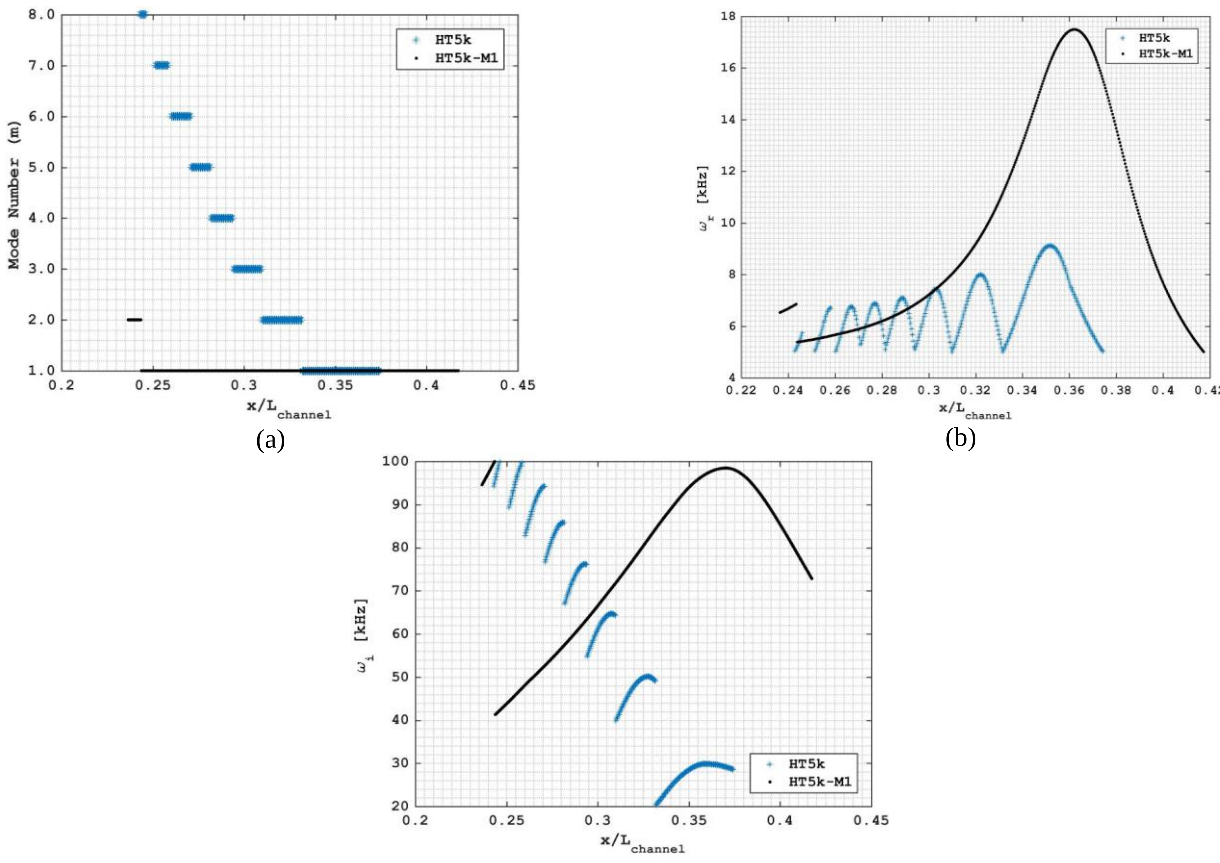

Figure 11: Comparison of the predicted low-frequency modes in the ionization region of the HT5k and HT5k-M1, (a) wave number along the x-direction, (b) ω_r along x-direction, (c) ω_i along x-direction. The $L_{channel}$ is the channel length of the HT5k-M1.

Interesting comparisons can also be made between the HT5k and M1 thrusters regarding the plasma stability in the high-frequency range by referring to Figure 12. As a matter of fact, in the HF range, the dominant axial modes have always the wave numbers of either -100 or -500 m^{-1}. Nevertheless, the k = -100 m^{-1} modes are dominant over a broader extent of the acceleration zone in the HT5k compared to M1. In HT5k-M1, the unstable modes of either wave numbers occur over an almost equal total axial extent of the acceleration region, but with the k = -500 m^{-1} modes being slightly more prevalent.

Despite the similarity in the wave numbers of the dominant axial modes, the instabilities show notably different frequency and growth rate characteristics. In terms of the growth rate, the modes in M1 configuration has generally larger imaginary frequency components, with the difference reaching up to about 150 kHz. As it regards the real frequency, although the axial modes have initially quite similar frequencies, beyond the HT5k-M1 exit plane, the frequency increases up to about 5MHz whereas the modes in HT5k persistently have frequencies in the range of few hundreds of kHz even beyond the exit plane. Analyzing the dispersion relation of the general two-stream instabilities, and deriving the correlation between the frequency, growth rate and the plasma parameters following the approach in Ref. 20, it was noticed that the frequency and growth rate of the modes are proportional to the axial derivative of the ion beam velocity (dV_i/dx). Since, due to the change in the topology of the magnetic field, the gradient of ion flow velocity is larger in HT5k-M1 than in HT5k, the axial modes consistently demonstrate larger frequencies and growth rates in M1 thruster.

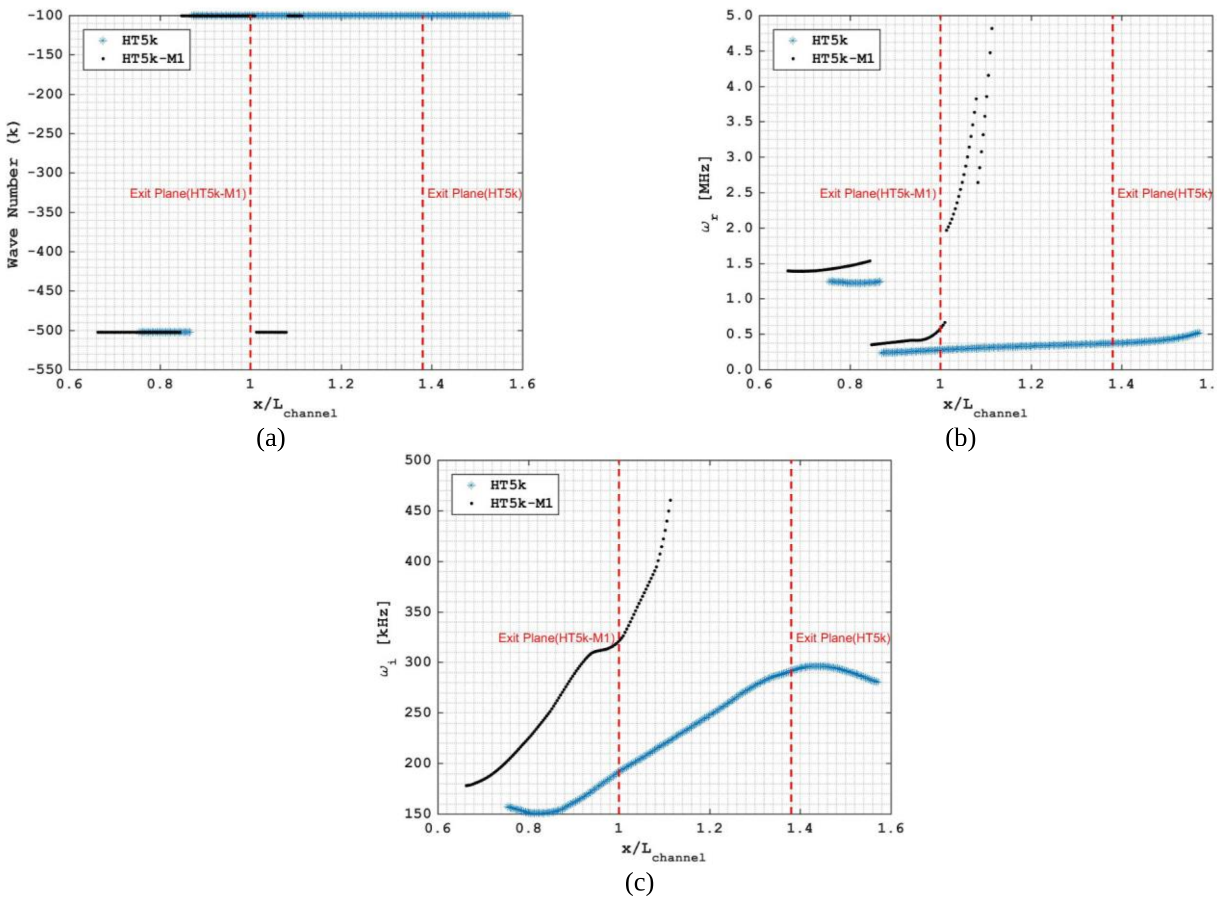

Figure 12: Comparison of the predicted high-frequency modes in the acceleration region of the HT5k and HT5k-M1, (a) wave number along the x-direction, (b) ω_r along x-direction, (c) ω_i along x-direction. The $L_{channel}$ is the channel length of the HT5k-M1.

D. Preliminary MICaPS Results: Verification of the UATC Assumptions on Instabilities' Characteristics

A main purpose behind the development of the Stability Analysis Module was to obtain a more self-consistent description of the instabilities and their characteristics as the inputs of the UATC module. At the moment, the SAM formulation allows characterization of the unstable modes in the ionization and acceleration regions with acceptable accuracy. As a result, to present the preliminary results of MICaPs, we compare the characteristics of the unstable modes in these two regions, obtained using the plasma properties from the Complemented Code (Baseline plus UATC), against the assumptions on the wave properties initially included in the UATC. Finally, we also present a comparison between the profile of the instability-induced collision frequency in two cases corresponding to before and after the application of the SAM results in the UATC.

Figure 13 shows the variations along the axial direction of the mode number, frequency and growth rate of the low-frequency modes in the HT5k using the plasma profiles from the Complemented Code. In addition, Figure 14 shows the change in the properties of the high-frequency unstable modes in the HT5k along the x-direction using the same input data. Comparing Figure 13 with Figure 7, it is evident that in the ionization zone, apart from minor differences in the extent of existence of spoke modes, the characteristics of the unstable waves are very similar using either the Bohm or instability-induced description for the transport in the ionization region.

Nevertheless, looking at Figure 14 and Figure 9, it is clear that, as expected in the acceleration region, a more accurate description of transport mechanism as given by UATC, results in notably different properties of the axial wave modes of the same wave number. In fact, the characteristics of the unstable modes obtained using the data from the Complemented Code are more closely in line with the beam-plasma instability characteristics[9,30].

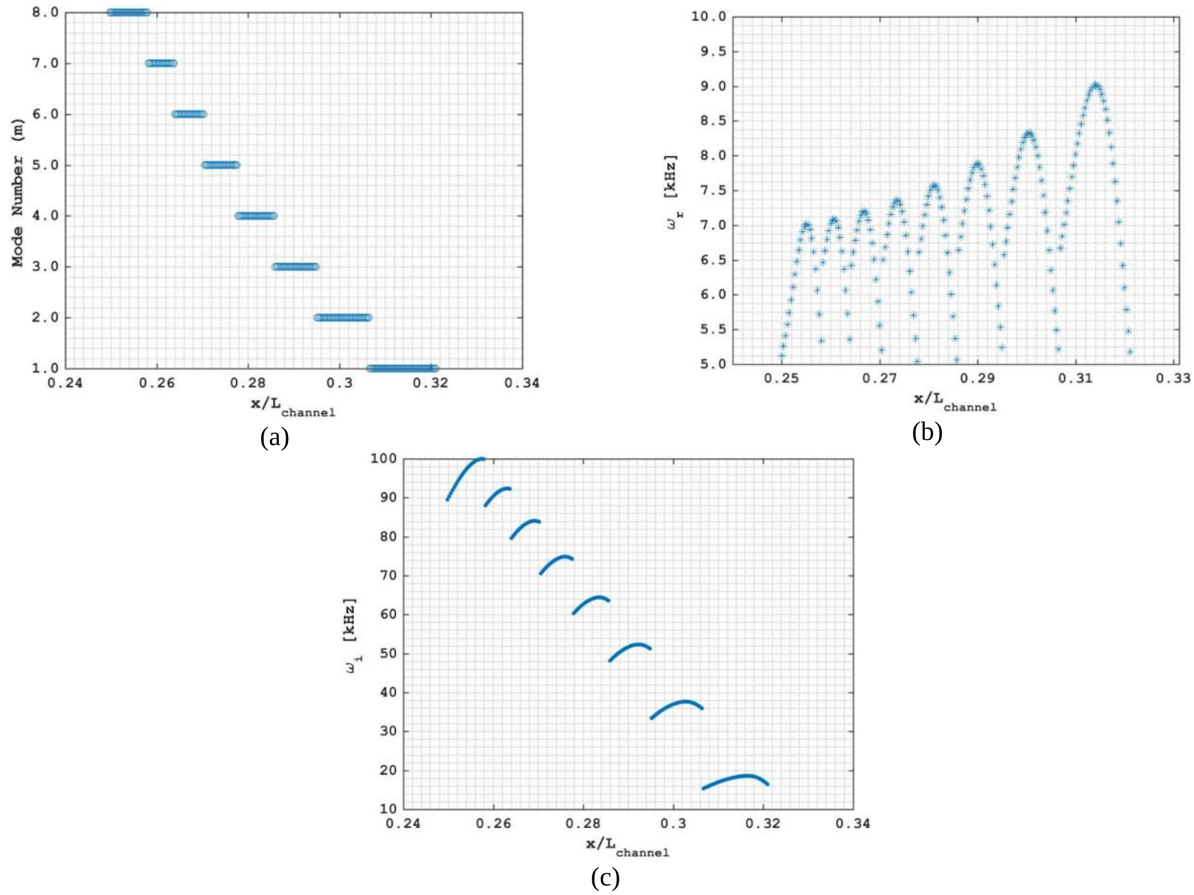

Figure 13: Characteristics of the low-frequency modes in the ionization region of the HT5k using Complemented Code Profiles, (a) mode number along the x-direction, (b) ω_r along x-direction, (c) ω_i along x-direction. The $L_{channel}$ corresponds to the channel length of the HT5k-M1.

Concerning the verification of the UATC assumptions on wave properties, the SAM results confirm that the characteristics of the unstable modes are consistent with the values of the instability parameters originally included. As it regards the spoke instability, a main difference is related to the fact that there is a distribution in the mode number of the fastest-growing mode along the axial direction. In contrast, in the UATC, it was originally assumed that the strongest spoke mode has a mode number of m = 5 over the entire ionization region.

In the acceleration region, we had considered initially that axially-unstable modes corresponding to the beam-plasma instability excite inside the channel, around the beginning of the acceleration zone, and propagate axially outward towards the plume, in the same direction as the propagation of transit-time instabilities. Under this assumption, the values of the beam-plasma wave properties used in UATC are, to a great extent, consistent with the predictions of instability characteristics from SAM. As a matter of fact, in UATC, the wave number at the excitation location has been assumed to be 450 m^{-1} and the wave frequency to be about 3 MHz. The SAM results show the absolute k value of 500 m^{-1} and the frequency of about 1 MHz, which demonstrate good agreement between the UATC "a priori" inputs and resolved instability properties in the acceleration region.

However, noting that the current results show the propagation of the instability waves towards the anode, changing the assumption on the excitation location in UATC from the beginning to the end of the acceleration region implies notable differences in the wave properties. This is because near the end of the region, SAM predicts waves with the absolute k value of 100 m^{-1} and the real frequency of about 800 kHz. The results of the incorporation of these SAM outputs in

UATC and the implications of changes in the profile of the instability-induced collision frequency (Figure 15) are discussed in the following paragraphs.

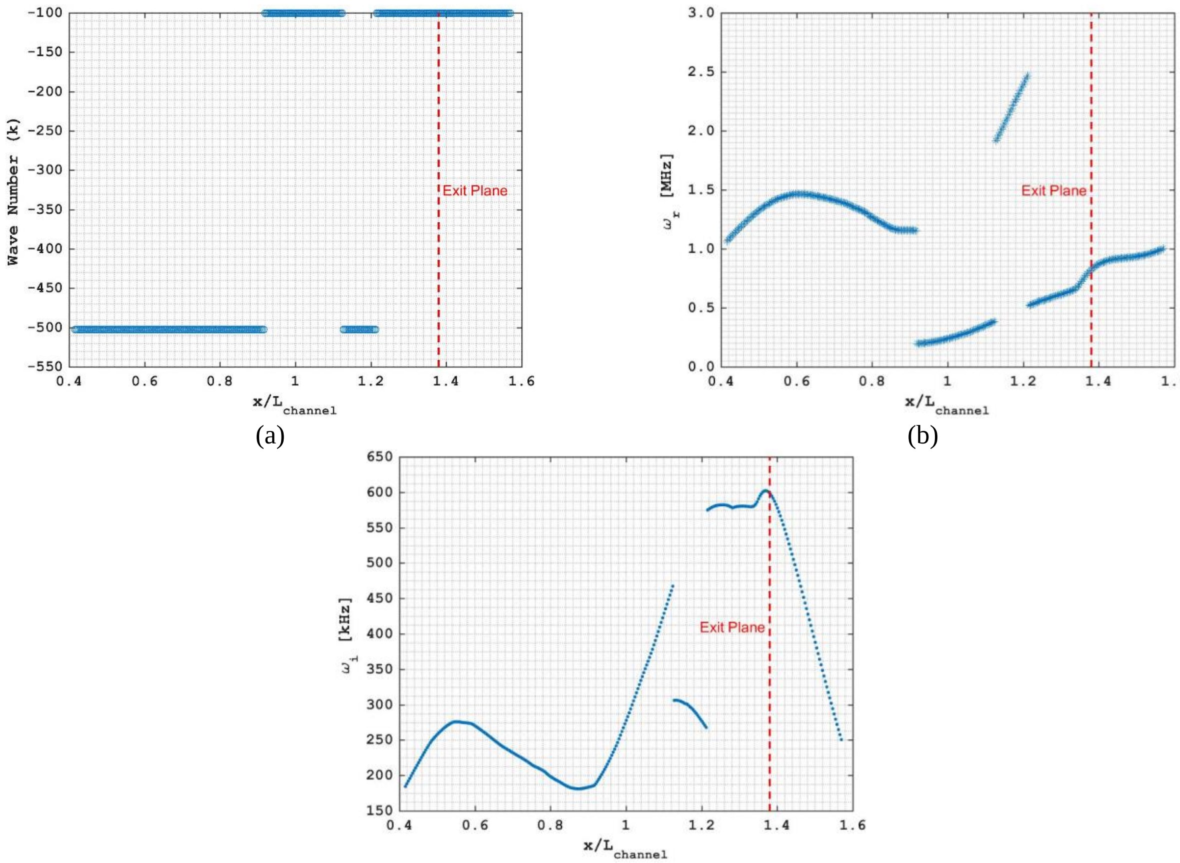

Figure 14: Characteristics of the high-frequency modes in the acceleration region of the HT5k using Complemented Code Profiles, (a) mode number along the x-direction, (b) ω_r along x-direction, (c) ω_i along x-direction. The $L_{channel}$ corresponds to the channel length of the HT5k-M1.

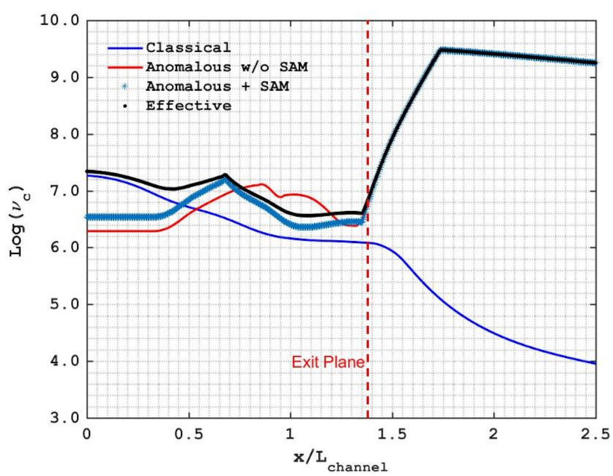

Figure 15: Comparison between the profiles of the instability-induced collision frequency (υ_c) from UATC before (red line) and after the incorporation of the SAM results (blue asterisks); also shown are the classical and the effective collision frequencies. The $L_{channel}$ corresponds to the channel length of the HT5k-M1.

Figure 15 presents the distribution of various collision frequencies along the channel centerline of the HT5k thruster. In particular, the red line corresponds to the anomalous collision frequency obtained from UATC with "a priori" assumption of the wave properties whereas the curve with blue asterisks represent the variations in instability-induced collision frequency after the inclusion of SAM outcomes. Furthermore, the black line shows the effective collision frequency defined as the sum of the classical collision frequency and the anomalous one.

Referring to Figure 15, the incorporation of the SAM predictions inside the channel in the UATC module has resulted in two primary changes. First, noting that the spokes are now considered to contribute to transport up to approximately where SAM predicts their existence, and that the acceleration region has been extended further inward, the peak in anomalous collision frequency have shifted towards the anode. Second, having now considered in UATC that the beam-plasma waves are propagating from the end of the acceleration region inward with the characteristics obtained from SAM, the curvature of the υ_c profile changes in this region. However, in terms of the magnitude, the υ_c values before and after the SAM integration are still on the same order throughout the domain.

The value of the collision frequency from UATC near the exit, about the location of maximum magnetic field intensity along the centerline, is the same for both cases of with and without SAM. Nevertheless, for the case with SAM results, the collision frequency remains almost constant up to $x/L_{channel}$ of about 1. The effects of this difference can be considerable on the distribution of plasma parameters, particularly the plasma potential, since we have observed that the relatively-low effective collision frequency in the acceleration region near the so-called "dip" location can result in unrealistic numerical solution for potential drop by the baseline[11,20]. However, as it was speculated in our previous work, it is probable that the beam-plasma instability, with the assumed wave electric field amplitude at saturation, be insufficient to fully explain the anomalous transport in the acceleration region. As a matter of fact, since the MICaPS code at its current stage of development does not allow resolving time-varying and nonlinear phenomena, it is not possible to self-consistently obtain this kind of information. As a result, the significance of the beam-plasma instability to cross-field current conduction remains an open point that merits further investigation through future upgrades of the MICaPS scheme.

IV. Conclusions and Future Work

In this paper, a novel framework was presented to address the problem of anomalous cross-field electron transport in Hall thrusters within the context of a modular comprehensive code (MICaPS). The general idea behind the MICaPS is to divide the fluid simulation of Hall thruster plasma into one main solver of the plasma system of equations, and the modules that predict the characteristics of the current-carrying instabilities and correlate their properties to instability-induced cross-field axial electron current. Noting the significantly-complex and multiscale nature of the turbulence in Hall thruster plasma, this approach allows investigating the level of accuracy and detailedness of the physical models of the transport mechanisms, which are necessary to acquire descriptions that capture accurately-enough the underlying physics of the phenomena involved. The modularity of the scheme also provides the opportunity to understand the improvements required in each module in view of augmenting the physical representativeness and accuracy of others such that the entire MICaPS code eventually approaches the level of predictivity.

Apart from introducing the MICaPS framework, the remaining of this work was dedicated to the presentation of the developed Stability Analysis Module. The derivation of the system of linearized perturbed equations for the ions and electrons, and the implications and limitations of the followed stability analysis approach, were extensively discussed. Additionally, the results of the module application to characterize low- and high-frequency instabilities in the ionization and acceleration regions of two different thrusters were discussed. Finally, preliminary MICaPS results were presented in terms of verifying the UATC assumptions on the instability waves characteristics and investigating the changes in the UATC outcome by incorporating SAM results.

As already noted above, all three MICaPS modules have ample room for improvements, and the work is currently ongoing in this regard. In particular, concerning the baseline module, extensive research is being pursued within the framework of a doctorate dissertation on further advancing the quasi-2D fluid simulation [17]. This effort aims at increasing the accuracy of the physical descriptions, the reliability of the numerical scheme, and allowing to assess non-stationary plasma response.

Besides, efforts are in parallel ongoing to augment the capabilities of the SAM module with respect to the study of axial instabilities, and to update its formulation so as to be able to characterize the high-frequency short-wavelength instabilities in the near-plume region. Finally, regarding the UATC, the closure model corresponding to the beam-plasma instability, in particular, and the numerical robustness of the code, in general, are being improved.

Acknowledgments

The authors are greatly thankful of Professor Mariano Andrenucci for his supports and insights. In addition, we would like to appreciate the efforts of Vittorio Giannetti in setting the foundation of the baseline model and his constant contributions to its development. We also thank Manuel Saravia and Vittorio Giannetti for the fruitful discussions.

References

[1]P. Coche and L. Garrigues, "A two-dimensional (azimuthal-axial) particle-in-cell model of a Hall thruster", *Phys. of Plasmas*, 21, 023503, 2014

[2]V. Croes, T. Lafleur, Z. Bonaventura, A. Bourdon and P. Chabert, "2D particle-in-cell simulations of the electron drift instability and associated anomalous electron transport in Hall-effect thrusters", *Plasma Sources Sci. Technol.* 26, 034001 (14pp), 2017

[3]S. Janhunen, A. Smolyakov, O. Chapurin, D. Sydorenko, I. Kaganovich, and Y. Raitses, "Nonlinear structures and anomalous transport in partially magnetized ExB plasmas", *Physics of Plasmas* 25, 011608 (2018); doi: 10.1063/1.5001206

[4]J.P. Boeuf, "New insights from PIC simulations on the EXB Electron Drift Instability in Hall thrusters", IEPC-2017-216, *Presented at the 35th International Electric Propulsion Conference Georgia Institute of Technology*, Atlanta, Georgia, USA October 8 – 12, 2017

[5]A. Lazurenko, L. Albarède, A. Bouchoule, "High-frequency Instabilities in Hall-effect Thrusters: Correlation with the Discharge Current and Thruster Scale Impact", IEPC-2005-142, *Presented at the 29th International Electric Propulsion Conference, Princeton University,* October 31 – November 4, 2005

[6]S. Tsikata, A. Heron, C. Honore, "Oscillatory discharge behavior in Hall thrusters: relationships between the discharge current, electric field and microturbulence", *Presented at the 35th International Electric Propulsion Conference Georgia Institute of Technology*, Atlanta, Georgia, USA October 8 – 12, 2017

[7]A. Heron and J. C. Adam, Anomalous conductivity in Hall thrusters: "Effects of the non-linear coupling of the electron-cyclotron drift instability with secondary electron emission of the walls", *Phys. of Plasmas* 20, 082313, 2013

[8]S. Yoshikawa, and D.J. Rose, "Anomalous Diffusion of a Plasma across a Magnetic Field," *Physics of Fluids*, Vol. 5, 1962, pp.334

[9]C.A. Thomas, N. Gascon, M. Allis, E. Sommier, and M.A. Cappelli, "Non-local electric field effects in magnetized plasmas", IEPC-2005-028, *Presented at the 29th International Electric Propulsion Conference, Princeton University*, October 31 – November 4, 2005

[10]T. Lafleur, S.D. Baalrud, P. Chabert, "Theory for the anomalous electron transport in Hall effect thrusters. II.Kinetic model", *Physics of Plasma*, 23, 053503, 2016

[11]M. Reza, F. Faraji, T. Andreussi, M. Andrenucci, "A Model for Turbulence-Induced Electron Transport in Hall Thrusters", IEPC-2017-367, *Presented at the 35th International Electric Propulsion Conference Georgia Institute of Technology*, Atlanta, Georgia, USA October 8 – 12, 2017

[12]A.L. Ortega, I. Katz, V.H. Chaplin, "A First-Principles Model Based on Saturation of the Electron Cyclotron Drift Instability for Electron Transport in Hydrodynamics Simulations of Hall Thruster Plasmas", IEPC-2017-178, *Presented at the 35th International Electric Propulsion Conference Georgia Institute of Technology*, Atlanta, Georgia, USA October 8 – 12, 2017

[13]B. Jorns, "Predictive, data-driven model for the anomalous electron collision frequency in a Hall effect thruster", *Plasma Sources Sci. Technol.* 27 (2018) 104007 (14pp)

[14] I. Katz, V.H. Chaplin, A.L. Ortega, "Particle-in-cell simulations of Hall thruster acceleration and near plume regions", PHYSICS OF PLASMAS 25, 123504 (2018)

[15]K. Hara, K. Kubota, "Direct kinetic simulation of ion acoustic turbulence in cathode plume", IEPC-2017-496, *Presented at the 35th International Electric Propulsion Conference Georgia Institute of Technology*, Atlanta, Georgia, USA October 8 – 12, 2017

[16]V. Giannetti, T. Andreussi, A. Leporini, D. Estublier, and M. Andrenucci, "Long-Life Low Erosion Hall Effect Thruster: Model and Simulations", *In proceedings of the 5th Space Propulsion Conference*, Rome, Italy, May 2016, paper SP2016_3125199

[17]V. Giannetti, A. Leporini, T. Andreussi, and M. Andrenucci, "Theoretical Investigation of a 5 kW Class Hall Effect Thruster". *In proceedings of the 34th International Electric Propulsion Conference*, Hyogo-Kobe, Japan, July 2015, paper IEPC-2015-212.

[18]T. Andreussi, V. Giannetti, A. Leporini, M.M. Saravia, and M. Andrenucci, "Influence of the magnetic field configuration on the plasma flow in Hall thrusters", *Plasma Phys. Control. Fusion* 60 (2018) 014015 (16pp)

[19]F. Taccogna, S. Longo, M. Capitelli, and R. Schneider, "Seven years of Hall thruster modeling: An European collaboration between Bari and Greifswald", IEPC-2007-12, *Presented at the 30th International Electric Propulsion Conference*, Florence, Italy September 17-20, 2007

[20]F. Faraji, M. Reza, "Investigation and Modeling of Turbulence-Induced Electron Cross-Field Transport in Hall Thrusters", Master's dissertation, *University of Pisa*, 2017

[21]R Kawashima, K Hara, and K Komurasaki, "Numerical analysis of azimuthally rotating spokes in a crossed-field discharge plasma", Submitted to: *Plasma Sources Sci. and Technol.*

[22]T. Andreussi, V. Giannetti, A. Leporini, C. Ducci, D. Estublier, C. Edwards, A. Rossodivita, and M. Andrenucci, "Temporal Evolution of the Performance and Channel Erosion of a 5kw-Class Hall Effect Thruster Operating with Alternative Propellants". SP2016_3125164, *In Proc. Space Propulsion Conference*, 2016

[23]V. Giannetti, A. Leporini, M. Andrenucci, and T. Andreussi, M.M. Saravia, D. Estublier, "Theoretical and Experimental Investigation of Low-Erosion Hall Thruster Configurations", IEPC-2017-395, *Presented at the 35th International Electric Propulsion Conference Georgia Institute of Technology*, Atlanta, Georgia, USA October 8 – 12, 2017

[24]M.S. McDonald and A.D. Gallimore, Parametric investigation of the rotating spoke instability in Hall thrusters, *Phys. of Plasma*, 242, 2011

[25] J.P. Boeuf, "Rotating structures in low temperature magnetized plasmas--insight from particle simulations", *Frontiers in Physics*, 2014, doi: 10.3389/fphy.2014.00074.

[26] G.S. Janes and R.S. Lowder, "Anomalous Electron Diffusion and Ion Acceleration in a Low-Density Plasma", *Phys. of Fluids* 9, 1966

[27]M.J. Sekerak, "Plasma Oscillations and Operational Modes in Hall Effect Thrusters", Ph.D. Dissertation, *University of Michigan*, 2014

[28]A. Lazurenko, L. Albarède, A. Bouchoule, "Physical characterization of high-frequency instabilities in Hall thrusters", *PHYSICS OF PLASMAS* 13, 083503, 2006

[29]S. Barral, K. Makowski, Z. Peradzynski and M. Dudeck, "Transit-time instabilities in Hall thrusters", *Phys. of Plasmas*, 12, 073504, 2005

[30]C.A. Thomas and M.A. Cappelli, "Gradient transport processes in E×B plasmas", *41st AIAA/ASME/SAE/ASEE Joint Propulsion Conference & Exhibit*, 10 - 13 July 2005, Tucson, Arizona

[31]C.A. Thomas, "Anomalous electron transport in the Hall-effect thruster", Ph.D. Dissertation, *Stanford University*, 2007

[32]D. Escobar, E. Ahedo, "Analysing the azimuthal spoke oscillation of Hall thrusters via numerical simulation", *AIAA/ASME/SAE/ASEE Joint Propulsion Conference*, 2014